energy&fuels

pubs.acs.org/EF Article

Detailed Characterization of Vitrinite-Rich Subbituminous and Bituminous Coals for Utilization in Carbon Fiber Precursor Production

Ercan Cakmak,* Jonathan P. Mathews, Sungsool Wi, Matthew R. Ryder, Martha Chacón-Patiño, Amy M. McKenna, Frederic Vautard, Mark Arnould, Harry Meyer, III, and Edgar Lara-Curzio

Cite This: https://doi.org/10.1021/acs.energyfuels.3c05200 Read Online

ACCESS | Metrics & More | Article Recommendations | Supporting Information

ABSTRACT: Chemical structures of candidate coals (one subbituminous coal from the Powder River Basin and three bituminous Eastern US coals) were examined for potential low-cost carbon fiber precursor production. The structural evaluation examined the carbon skeleton (^{13}C nuclear magnetic resonance (NMR) and high-resolution transmission electron microscopy (HRTEM)), the heteroatom functionality (X-ray photoelectron spectroscopy (XPS) Fourier transform infrared spectroscopy (FTIR) and NMR), the structural ordering and distribution of PAH sizes (HRTEM), and an estimation of the molecular weight distribution (laser desorption ionization mass spectrometry, LDIMS). The molecular compositional distributions were also evaluated for a mixed solvent extract (atmospheric pressure photoionization, 21 T Fourier transform ion cyclotron resonance mass spectrometry, FT-ICR MS). Significant structural differences existed between the subbituminous and bituminous coals, as expected with coalification (with the bituminous coals having a higher carbon content, lower oxygen content, higher aromaticity values, larger cluster sizes, and so forth). While the bituminous coals were similar in structure (close in rank with Blue Gem being hvAb and the rest being hvBb), structural differences were still evident. Specifically, structural similarities were evident for the average properties of Herrin and Springfield coals: same rank, similar moisture, and volatile matter yields, along with similar aromaticity and carbon and hydrogen content. However, significant structural differences were observed at the molecular level by 21 T FT-ICR MS, which showed that the Springfield coal was structurally more complex. Specifically, 21740, 16931, 30190, and 12982 unique elemental compositions were identified for the Monarch, Herrin, Springfield, and Blue Gem coals, further illustrating the complexity of the coal.

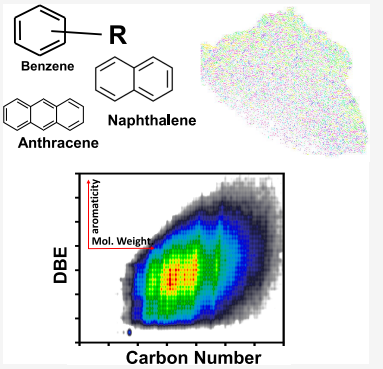

1. INTRODUCTION

Coal is a highly heterogeneous and complex natural material extensively used in power generation. It is a nationally and regionally important commodity in the United States, home to the largest coal reserves.[1] While coal is abundant domestically and is widely distributed,[2] due to CO_2 emissions and the associated climate change, the use of coal for electricity generation is being phased out domestically and in many other nations. Alternative uses are thus desirable, such as precursor production for higher value-added products for regional and U.S. economic development.[3]

Low-density, high-strength carbon fibers are attractive, high-value products with strategic commercial importance. Inexpensive carbon fibers are necessary to enable the clean energy transition (fuel-efficient vehicles, improved wind turbine blades, hydrogen transportation/storage, and batteries); there are also challenges with the large-scale supply of carbon fiber precursors. A research partnership between Oak Ridge National Laboratory (ORNL), the University of Kentucky, and Pennsylvania State University was formed to investigate the potential use of coal as a carbon fiber precursor. Such multi-institute effort was critical for this simple yet challenging task necessitated by the complex heterogeneous nature of coal, constituting both organic and inorganic phases.

To further elaborate the complexity of the work, to make high quality carbon fibers with high mechanical performance, the melt spinning of mesophase pitch has to be considered (isotropic pitch will result in low mechanical performance, even with little defects). The precursor must then be suitable to produce a mesophase pitch with large flow domains (as opposed to mosaic domains). Previous work showed that a large molecular weight distribution is better (lower molecular weight components allowing the viscosity of the media to stay low enough for the larger polyaromatic molecules to

Received: January 9, 2024
Revised: March 11, 2024
Accepted: March 15, 2024

condensate and diffuse, leading to the liquid crystal structure of the mesophase).[4] Also, previous work from ORNL showed that methyl groups on the edge of the molecules are necessary for the orientation to occur.[5] Purely cata-condensed molecules with no pendant aliphatic chains are therefore not suitable for producing good quality mesophase. In order to be processed with melt spinning, the softening point of the mesophase pitch should not be too high (<300 °C is better), in order to avoid condensation reactions and too much volatilization in the extruder. This again is a function of the presence of aliphatic chains and bridges in the molecular components, as well as of the molecular mass distribution (a low molecular weight fraction is needed, but it needs to be part of a continuous distribution). Further, the concentration in heteroatoms (particularly sulfur) needs to be limited (a few at % at the most), which can prevent the generation of mesophase at high concentrations. Finally, the inorganic phase (ash) needs to be removed as much as possible, as it will form defects in the carbon fiber.

Four candidate coals were selected for examination: three bituminous coals from the Appalachian and Illinois Basins and one subbituminous coal from the Powder River Basin. These coals have already been characterized in detail by our group, and there is extensive data on the porosity, pore size distribution, and pore accessibility,[6] as well as the physical structure (composition, petrology, and the 3D spacing of lithotypes and minerals), the digestion behavior (extract yields and temperature relationships) along with quinoline soluble liquid yields),[7] and simulations data (atomistic representations with extraction simulations).[8] However, to relate the desirable chemical structural features in coal to the desirable carbon fiber precursors, it is necessary to go beyond average values, delving into the structural feature distributions. This requires combined data sets obtained through various advanced analytical techniques.

Traditionally, proximate, ultimate, and coal petrology are the fundamental analyses required for establishing basic properties and coal rank, useful as indicators for expected behavior. However, the complexity of coal rank, compounded by maceral and mineral compositional differences, can yield different behaviors for coals with apparently similar basic properties. A deeper dive into the structural variations requires analysis of the heteroatom compositional contributions and polyaromatic hydrocarbon base structure distributions, and the diversity of structural features across the broad molecular weight distribution is required.

The heteroatoms are a significant contribution for low-rank coals into the bituminous range, and the composition can be elucidated by chemical or spectroscopy approaches. Fourier transform infrared spectroscopy (FTIR) is commonly employed in heteroatom characterization, and while semi-quantitative, the measurements are quick with minimal sample preparation. The data can provide estimates for the aromatic to aliphatic carbon ratio, oxygen functionalities, degree of maturation/aromatic ring condensation, and the aliphatic chain length/degree of branching.[9−13]

For elucidation of the carbon skeletal structure distributions, solid-state $^{1}H-^{13}C$ cross-polarization magic-angle spinning (CPMAS) nuclear magnetic resonance (NMR)[10] is the gold standard. Coal has a distribution of single to multifused aromatic rings with side-chain attachments and cross-links (via heteroatom, aliphatic structures, or directly between aromatic carbons). Thus, this approach can quantitatively determine the types and distributions of aromatic and aliphatic carbons.[14,15] Solum et al.[13,16] performed groundbreaking work in this area that provides a comprehensive parameter set used to describe the skeletal structure.

While these spectroscopic techniques mostly provide average structural properties, structural distributions are also required to elucidate the relationship between structure and behavior. High-resolution transmission electron microscopy (HRTEM) is well-established to explore coal structures.[17,18] The micrographs can be processed to extract the lattice fringes (the edge in view of the aromatic structures that are in focus in a thin (transmission) region). Further image analysis provides the distribution of lattice fringe lengths, the orientation, and for coals with higher levels of ordering, *d*-spacing equivalents, the stacking extent, and curvature analysis.[19−21] For example, low-rank coals have short fringes, with limited orientation and stacking.[18,19] The fringe length distributions change slightly with rank (and maceral influences[18]) until low volatile bituminous to anthracite ranks, where longer fringes are present with increasing frequency.[19] Assumptions for the ring catenation permit the PAH distributions to be estimated,[22] and with image-guided construction approaches,[23] these PAH distributions and ordering can be generated in atomistic "slice" representations.[21,22,24,25] The generated atomistic representations can further be cross-linked, and heteroatoms can be added to provide small- to large-scale structural representations for atomistic simulations. The cross-linking extent can be estimated by combining the NMR data with an estimate of the molecular weight distribution by laser desorption mass spectroscopy (LDIMS).[26] Laser desorption ionization (LDI) and matrix-assisted LDI (MALDI) MS techniques have been used in coal and coal products to examine masses of up to 270,000 m/z.[27,28]

These techniques combined provide a solid base for constructing small-scale representations of coal. However, an additional technique permits the consideration of the structural complexity by examining the elemental composition of the individual (ionized) molecules. This requires a high mass resolving power to distinguish species separated by an electron mass.[29] The ultrahigh resolution 21 T Fourier transform ion cyclotron resonance (FT-ICR) MS system in the Maglab of Florida State University can separate and identify individual molecular ions that differ by roughly the mass of an electron, with a mass resolving power of $m/\Delta_{m50\%}$ of >3,000,000 at m/z 200[30] ($\Delta_{m50\%}$= mass spectral peak full width at half-maximum peak height) and mass accuracy of <30−60 ppb.[31−33] With unparalleled ultrahigh resolving power, the elemental compositions can be assigned based on Kendrick mass sorting of mass-to-charge ratios from ionized analyte molecules.[34] Previous studies reported detecting up to 10,000,[31] 30,000,[35] 50,000,[36] and even over 85,000[37] compositionally distinct species from coal and petroleum components (albeit that these are solvent extractable molecules).[31,32,34,38−41] The molecular distributions are presented as isoabundance plots, providing an unprecedented molecular-level compositional insight into the coal structure and potentially providing insight into the desirable molecular characteristics for carbon-fiber precursors and aiding elucidation for behavior differences of apparently similar coals.

Detailed and representative molecular information is crucial for constructing atomistic representations that capture the behaviors required for processing and industrial utilization pathways. Here, we present a comprehensive chemical data set

https://doi.org/10.1021/acs.energyfuels.3c05200
Energy Fuels XXXX, XXX, XXX−XXX

for three industrially relevant bituminous and one subbituminous coal, obtained using NMR, HRTEM, LDI MS, FTIR, X-ray photoelectron spectroscopy (XPS), and FT-ICR MS techniques. These data are the basis for a discussion of the suitability of these coals for the production of carbon fiber precursor production. These data will also be used in the construction of large-scale complex atomistic representations to be presented in a separate publication.

2. EXPERIMENTAL SECTION

2.1. Coals. Coals were selected from three basins: a subbituminous (Monarch) coal from the Powder River Basin, two bituminous coals (Herrin and Springfield) from the Illinois Basin, and one (Blue Gem) from the Central Appalachian Basin. Coals were selected from working mines with abundant reserves, so a significant supply could be available should the carbon fiber research prove successful. Within the selected coals, Blue Gem prompted initial interest due to its exceptionally low ash yield (~1 wt %). The Herrin and Springfield samples represent more abundant sources and are close in rank to Blue Gem. The Monarch sample was selected due to its exceptionally low sulfur content and to represent abundant low-rank coal. No special handling was performed for the low-rank Monarch coal.

Within the studied set, the rank order (lowest to highest) is Monarch, Herrin, Springfield, and Blue Gem based on vitrinite reflectance values (R_0, max) of 0.39, 0.65, 0.67, and 0.88%, respectively.[6] Both raw and demineralized coals were used in this work. More details are given in our previous publications[6,7] and are omitted here to avoid duplication.

2.2. FTIR Measurements and Data Fitting. Demineralized coal samples were ground with potassium bromide (KBr) at a concentration of 50 vol % with a pestle and mortar, and 1 mm pellets were made using a Carver hydraulic press (pressure of 4 tons). A PerkinElmer Frontier FTIR spectrometer was used in the attenuated total reflection (ATR) mode. The background and the sample spectra were generated by cumulating 16 scans over a wavenumber range of 400 to 4000 cm^{-1} with an accuracy of 2 cm^{-1}. The baseline of all spectra was manually corrected.

2.3. Solid-State ^{13}C NMR Measurements. The solid-state $^1H-^{13}C$ cross-polarization magic-angle spinning (CPMAS) NMR spectra of the demineralized coal samples were recorded by using a custom-built 3.2 mm ^1H-X-Y triple resonance MAS probe on a 14.1-T magnet spectrometer (^1H 600 MHz) operated by a Bruker Avance III console at the MagLab of Florida State University. About 40 mg of each powdered coal sample was packed into the rotor and spun at 16 kHz. The pulse powers used in the experiment for the 90° pulses were 50 and 100 kHz, respectively, for the ^{13}C and ^1H channels. An optimal $^1H-^{13}C$ CP condition was found at ν_1 (^{13}C) = 50 kHz and ν_1 (^1H) ≈ 65 kHz while applying a rectangular pulse along the ^{13}C channel and simultaneously a ramped (70−110%) spin-lock pulse along the ^1H channel. The ^1H decoupling scheme applied during the direct and indirect acquisition periods of ^{13}C signals was SPINAL-64[42] with a decoupling rf power of 90 kHz. Two NMR experiments, variable contact $^1H-^{13}C$ CPMAS and dipolar dephasing experiments, were conducted for the fractional quantification of known carbon sites in the coal samples according to the method developed by Solum et al.[13] A total of 13 variable contact $^1H-^{13}C$ CPMAS experiments were obtained with variable contact times in the range of 0.5−10 ms for each sample for extracting the time constants of $^1H-^{13}C$ polarization transfer, T_{CH}, as well as the proton spin−lattice relaxation time, $T_{1\rho}^H$. Dipolar dephasing experiments were also conducted with 24 delay times in the range of 0−30 μs to extract the Lorentzian, Gaussian type of initial magnetizations, and decay constants of each spectrum peak component. These molecular parameters were employed to extract the fractional contents of the carbon sites.

2.4. HRTEM Measurements. The HRTEM micrographs were taken using an FEI Talos F200X scanning/transmission electron microscope equipped with a FEG source providing 0.12 nm resolution at the Materials Research Institute at The Pennsylvania State University. The samples were prepared by sonicating a small quantity of raw coal powder in ethanol for 5 min and then dropping 3−5 drops of the solution on copper-supported lacey carbon TEM grids. The instrument was operated at 200 kV, and micrographs were recorded in bright field mode at 630 kX magnification. Image processing and analysis were performed using Photoshop (to take advantage of the automation process for multiple micrographs). Here, 6 to 9 micrographs for each coal, selected from a larger pool of ~15 micrographs, were examined with the QIA plugin for processing and image analysis. Lattice fringe extraction was performed by using a Fourier transform filtering step with manual selection of the binarization threshold. Due to the field of view having regions too thick for transmission, a region of interest was manually selected after processing for analysis. Estimating the distribution of PAH sizes from the fringe lengths used the approach assuming a parallelogram catenation: benzene, naphthalene, phenanthrene, pyrene, and so forth.[22,25]

2.5. LDI-MS Measurements. LDI-MS measurements were performed at two separate institutions. The LDI-MS instrument used at The Pennsylvania State University was a Bruker Ultraflextreme MALDI-TOF equipped with a smartbeam-II IR laser (NdYAG), with a 2 kHz maximum repetition rate. The method parameters were optimized. Here, raw coal powders were used for the investigation. Repeat measurements were performed using demineralized coals at the Center for Nanophase Materials Sciences (CNMS), ORNL. The measurements were performed using Bruker Autoflex Speed MALDI-TOF equipment. Spectra were generated by summing 10000 laser shots into the sum buffer at 1000 shot intervals.

2.6. Twenty-One Tesla FT-ICR MS Measurements. The raw coal powders were extracted using a toluene/tetrahydrofuran/methanol mixture via Soxhlet extraction (5g for each coal). The yields for this extraction were 799, 983, 735, and 679 mg for the Monarch, Herrin, Springfield and Blue Gem coals, respectively. The extracted coal samples were further diluted in toluene to a final concentration of 100 μg/mL in HPLC grade toluene (Sigma-Aldrich Chemical Co., St. Louis, MO) prior to mass spectral analysis.

Each sample was diluted to yield a final concentration of 100 μg/mL in HPLS-grade toluene. The extracts were analyzed with a custom-built hybrid linear ion trap FT-ICR mass spectrometer equipped with a 21T superconducting solenoid magnet.[43] Samples were ionized with an Ion Maxx atmospheric pressure photoionization (APPI) source (ThermoFisher Corp., San Jose, CA, USA). Toluene is used as a solvent/dopant, to increase analyte ionization through dopant-assisted proton-transfer and charge-exchange reactions that are initiated by ionized toluene molecules at atmospheric pressure inside the ionization source in positive-ion mode.[44]

Positive-ion APPI (APPI+) is beneficial as it can ionize nonpolar compounds such as HC and basic N compounds as well as multiheteroatomic compounds (N_2, N_2O, NO, O, and S classes).[29,33,41,45] In this setup, the sample flows through the capillary at a rate of 50 μL/min and mixes with the nebulization gas (N_2, introduced at a pressure of 345 kPa, 16 mL/min) inside of a heated vaporizer operated at 350 °C. Once nebulized, the sample exits the vaporizer in a confined jet and flows under a krypton VUV gas discharge lamp that produces 10 eV photons (120 nm), where photoionization occurs at atmospheric pressure. Toluene ions are then swept into the heated metal capillary inlet of the mass analyzer. Ions were initially accumulated in an external multipole ion guide (1−5 ms) and released m/z-dependently by decrease of an auxiliary radio frequency potential between the multipole rods and the end-cap electrode.[46] Ions were excited to m/z-dependent radius to maximize the dynamic range and number of observed mass spectral peaks (32−64%),[47] and excitation and detection were performed on the same pair of electrodes.[48]

The dynamically harmonized ICR cell in the 21T FT-ICR is operated with 6 V trapping potential.[49] Time-domain transients of 3.1 s were conditionally coadded and acquired with the Predator data station that handled excitation and detection only, initiated by a TTL trigger from the commercial Thermo data station, with 100 time-domain acquisitions averaged for all experiments.[50] Mass spectra were

https://doi.org/10.1021/acs.energyfuels.3c05200
Energy Fuels XXXX, XXX, XXX−XXX

phase-corrected and internally calibrated with 10−15 highly abundant homologous series that spans the entire molecular weight distribution based on the "walking" calibration method.[51] Experimentally measured masses were converted from the International Union of Pure and Applied Chemistry (IUPAC) mass scale to the Kendrick mass scale[52] for rapid identification of homologous series for each heteroatom class (i.e., species with the same $C_cH_hN_nO_oS_s$ content, differing only by the degree of alkylation).[53] For each elemental composition, $C_cH_hN_nO_oS_s$, the heteroatom class, type (double bond equivalents, DBE = number of rings plus double bonds to carbon, DBE = $C - h/2 + n/2 + 1$),[54] and carbon number were tabulated for the subsequent heteroatom class relative abundance distributions and relative abundance weighted data being visualized. For each mass spectrum, more than 20,000 unique assignments corresponded to root-mean-square mass accuracy of less than 80 ppb. Peaks with signal magnitude greater than six times the baseline root-mean-square (rms) noise at m/z 500 were exported to peak lists, and molecular formula assignments and data visualization were performed with PetroOrg© software.[55] Molecular formula assignments with an error of >0.5 ppm were discarded. Only chemical classes with a combined relative abundance of ≥0.15% of the total were considered. The similarity between coal data sets was also compared to elucidate the structural similarities and differences. All FT-ICR MS files and elemental composition assignments are available via the Open Science Framework at https://osf.io/pt4un/ at DOI 10.17605/OSF.IO/PT4UN.

2.7. XPS Measurements. The XPS technique is used to determine the organically bound nitrogen and sulfur species.[11] The XPS was performed using a Thermo Scientific (Waltham, MA, USA) Model K-Alpha XPS instrument. The instrument utilizes monochromated, microfocused, Al Kα X-rays (1486.6 eV) with a variable spot size (i.e., 30−400 μm). Two areas were analyzed for each sample to gain insight into sample heterogeneity. The maximum X-ray spot size (400-μm diameter) was used to sample the largest area.

3. RESULTS AND DISCUSSION

3.1. Proximate, Ultimate, and Petrographic Analyses. The proximate and ultimate analyses and the maceral compositions of the investigated coals were presented in detail in previous work.[7] Some of these findings are presented in Table S1 and Supporting Information to provide relevant background for this work. According to the vitrinite reflectance values (R_0, max), the rank order was established as Monarch, Herrin, Springfield, and Blue Gem from low to high. However, all coals were high in vitrinite (84 to 91 vol % by point counting).

3.2. FTIR Spectroscopy. FTIR spectroscopy probed the chemistry and heteroatom functionality within the selected coal samples. The FTIR spectra, spanning from 4000 to 600 cm^{-1}, showed substantial similarity across all of the coals, indicating the presence of shared chemical structures and functional groups (Figure 1). Only minor unique features in each spectrum emphasized the presence of subtle compositional differences associated with the specific rank and geological origin. The Monarch coal showed the most significant difference, consistent with other characterization data. However, while more prominent in certain regions, such as the features around 1700 cm^{-1}, most are still present in the different samples and are shadowed by neighboring peaks. The features within the spectra were observed primarily as broad peaks, a characteristic reflection of complex, multicomponent systems. However, three spectral regions associated with various structural and functional groups are highlighted in Figure 1.

The 3200−3600 cm^{-1} region corresponds primarily to hydroxyl groups (O−H stretching) and suggests the presence

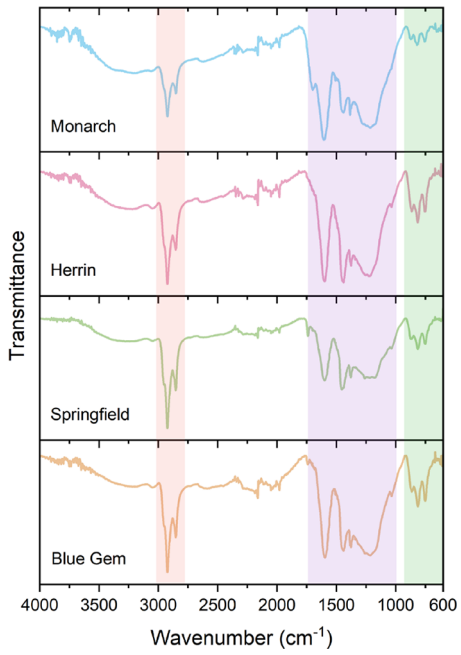

Figure 1. Fourier transform infrared (FTIR) spectra in the 4000−600 cm^{-1} range for four coal samples: Monarch, Herrin, Springfield, and Blue Gem. Regions associated with specific functional groups are highlighted, including C−H stretching (2800−3000 cm^{-1}), C−C and C−O stretching along with C−H bending (1000−1700 cm^{-1}), and aromatic ring deformations (600−900 cm^{-1}).

of residual moisture in the samples. The 2800−3000 cm^{-1} region, corresponding to aliphatic C−H stretching, revealed spectral features indicating aliphatic structures. The spectral region between 1000 and 1700 cm^{-1}, where C=O and C−O stretching is typically found, which displayed broad features indicating the likely presence of various oxygen-containing functional groups, such as carbonyl and ether. A small peak at approximately 1700 cm^{-1} in the Monarch coal sample suggests that it differs slightly from the others and could point to unique carbonyl functional groups such as carbonates, ketones, and quinones. However, it is essential to note that similar features are likely present in the other coals but obscured within broader spectral features in the different samples due to the complex nature of coals.

The 600−900 cm^{-1} region showed three distinct peaks. Given the inherent complexity, these peaks could represent aromatic ring deformations or a variety of overlapping absorption bands from the myriad of functional groups present. In addition to the identified features, certain spectral regions appeared to be noisy, which could be attributed to impurities or heterogeneity. The noisy region around ∼2500 cm^{-1} could be due to thiocyanate groups, and the features around ∼3600 cm^{-1} exhibited noise associated with the stretching vibrations of O−H or N−H groups, associated with increased oxygen content, moisture, or certain nitrogen-containing compounds.

While the features observed in the FTIR spectra are consistent with known trends in coal chemistry, the spectra of individual coals were not significantly different for the bituminous coals. However, as revealed in the following sections, significant differences exist at smaller length scales, adding to the complexity and microdiversity of functional groups in otherwise similar samples.

https://doi.org/10.1021/acs.energyfuels.3c05200
Energy Fuels XXXX, XXX, XXX−XXX

Table 1. Carbon Structural Parameters from Solid-State ^{13}C-NMR Measurements[a]

coal	f_a	$f_{a'}$	f_a^C	f_a^H	f_a^N	f_a^P	f_a^S	f_a^B	f_{al}	f_{al}^H	f_{al}^*	f_{al}^O
Monarch	0.67	0.63	0.04	0.23	0.40	0.04	0.16	0.20	0.33	0.19	0.14	0.06
Herrin	0.69	0.66	0.03	0.20	0.46	0.04	0.17	0.25	0.31	0.19	0.12	0.05
Springfield	0.69	0.65	0.04	0.22	0.43	0.04	0.15	0.24	0.31	0.19	0.12	0.05
Blue Gem	0.70	0.67	0.03	0.21	0.46	0.04	0.17	0.25	0.30	0.20	0.10	0.01

[a]Descriptions after ref 13. Fractions of sp^2-hybridized carbon: f_a = total carbon; $f_{a'}$ = in an aromatic ring; f_a^C = carbonyl (−CO_2), δ > 165 ppm; f_a^H = protonated and aromatic; f_a^N = nonprotonated and aromatic; f_a^P = phenolic or phenolic ether, δ = 150−165 ppm; f_a^S = alkylated aromatic, δ = 135−150 ppm; f_a^B = aromatic bridgehead; fractions of sp^3-hybridized carbon: f_{al} = total carbon; f_{al}^H = CH or CH_2; f_{al}^* = CH_3 or nonprotonated; f_{al}^O = bonded to oxygen, δ = 50−90 ppm.

3.3. Carbon Skeletal Structure Using ^{13}C Solid-State NMR. The 12 carbon structural parameters were obtained following the methodology of Solum et al.[13] are presented in Table 1. The relation between the various NMR parameters can be found in the original works.[13,16]

The coals have similarly corrected aromaticity values ($f_{a'}$) following the expected rank order of Monarch, Herrin, Springfield, and Blue Gem (0.63 to 0.67). The fraction of aromatic carbons is further divided into protonated (f_a^H) and nonprotonated (f_a^N) aromatic carbons. Because these values are inherently tied to aromaticity, comparing their relative values as a function of rank is appropriate. Typically, the ratio of the nonprotonated to protonated aromatic carbons increases with increasing vitrinite reflectance (rank).[12,56] While a clear-cut relation with rank is not observed within the limited rank range here, the lowest f_a^N/f_a^H value was for Monarch at 1.74, followed by Springfield (1.87), Blue Gem (2.19), and Herrin (2.42). Maceral differences will impact these data, with inertinite typically having a higher value than vitrinite.[57] However, Springfield coal has the higher inertinite contribution at 10% by volume (Table S1). A higher percentage of proton attachments (i.e., lower value of f_a^N/f_a^H) indicates a lower degree of connection between aromatic clusters.[56] This is thus expected to result in a higher frequency of smaller molecules/building blocks. Finally, for the fraction of aromatic bridgehead carbons (f_a^B), the bituminous coals effectively show the same fractions while the subbituminous Monarch coal has a lower value, indicating smaller aromatic clusters as expected.

The aliphatic structures in coal are in the form of side chains, cross-links, and hydroaromatic rings.[15] The fraction of aliphatic carbons, −CH_n, (f_{al}) are also presented in Table 1. The values follow the order of Monarch, Herrin/Springfield, and Blue Gem from highest to lowest but with subtle structural differences similar to the aromaticity values. The aliphatic carbon fraction can be further subdivided into methine/methylene (f_{al}^H) and methyl groups (f_{al}^*). While there is no significant difference between the coals regarding −CH/−CH_2 attachments, the fraction of −CH_3 attachments has a decreasing trend from Monarch to Blue Gem, consistent with coalification expectations (increasing aromaticity and gas generation).

Oxygen atoms are incorporated into the carbon skeletal structure in three forms: as carbonyl (f_a^C), open or closed phenolic ethers (f_a^P), or bonded to aliphatic side chains (f_{al}^O).[11,58] Table 1 does not show a particular trend with regard to carbonyl and ether attachments between the investigated coals. Nevertheless, the oxygen atoms bonded to aliphatic side chains reveal a decreasing trend from Monarch to Blue Gem. This agrees with the expected trend of abundant oxygen functionalities in low-rank coals.[59] The f_{al}^O data indicate that most oxygen atoms are combined with the carbon elements in the side chains (Monarch). With increasing coalification, the aliphatic side chains are gradually shorter, with select oxygen-containing groups undergoing thermolysis. As the degree of aromatic structure condensation increases, the hydrocarbon generation potential of the coal molecular structure gradually decreases. Further interpretation of the NMR data is possible following the work of Solum et al.[16] through which the derived lattice parameters are presented in Table 2.

Table 2. Carbon Lattice Parameters of Each Coal Following the Solum et al. Approach[16a]

coal	χ_b	C	σ+1	P_0	B.L.	S.C.	MW	M_δ
Monarch	0.32	14	4.4	0.30	1.3	3.1	495	72
Herrin	0.38	18	5.9	0.43	2.5	3.4	443	37
Springfield	0.36	17	4.8	0.37	1.8	3.0	394	39
Blue Gem	0.37	17	5.4	0.52	2.9	2.6	375	29

[a]Descriptions after ref 16 were χ_b is the ratio $f_a^B/f_{a'}$ and it is used to estimate the aromatic cluster size. The C is the number of carbon atoms per aromatic cluster. The σ+1 is the average number of attachments (bridges plus side chains) per cluster. The P_0 is the fraction of intact bridges. The B.L. is the number of bridges and loops per cluster, and S.C. is the number of side chains per cluster. The MW is the average molecular weight of a cluster (Da). Lastly, M_δ is the average molecular weight of a side chain or half of a bridge mass.

The χ_b parameter is used to characterize the degree of "polymerization" of the aromatic rings and is used to estimate the aromatic cluster size.[11,56] The three bituminous coals are characterized by similar aromatic cluster sizes with a lower value for the Monarch coal (Table 2). The number of carbon atoms per cluster, C, can then be calculated from the aromatic cluster size. The Monarch coal, on average, has 14 carbons per cluster corresponding to three fused aromatic rings. This is followed by 17−18 carbons in the bituminous coals, placing them slightly above pyrene (16 carbons).[13] The average aromatic carbon ring size increases with increasing maturation by combinations of cross-linking and aromatization of aliphatic carbon structures or aliphatic rings during maturation.[60] However, in the limited rank range examined here, the ring sizes are expected to be similar, as shown by the HRTEM data.[61]

The average number of attachments per cluster (σ+1) is subdivided into two groups: (1) bridges and loops and (2) side

https://doi.org/10.1021/acs.energyfuels.3c05200
Energy Fuels XXXX, XXX, XXX−XXX

chains. To elaborate, a connection between two different aromatic clusters is defined as a bridge, whereas a loop is formed when a bridge connects back to its originating cluster.[16] A side chain is an aliphatic chain assumed to terminate with a methyl group.[16,56] Through this reasoning, the fraction of intact bridges, P_0, can be calculated, which can then be used to calculate the average number of bridges and loops (B.L.) and side chains per cluster (S.C.).[16] The bridges and loops generally serve as a measure of the cross-linking between the aromatic clusters; however, the loops do not participate in cross-linking. The ratio of S.C. to B.L. can then be used to compare the coals. The lower values correspond to more frequent cross-linking between clusters. By this reasoning, the Monarch coal has the least cross-linked structures, while the Blue Gem coal has the most cross-linked structures.

Finally, the MW and M_δ values decrease with rank (from Monarch to Blue Gem). This aligns with the expected behavior where the cluster size grows (i.e., more places to attach side chains) with increasing rank but fewer attachment sites utilized due to reduced aliphatic content and loss of oxygen content.[13,56] At higher ranks (upper low volatile bituminous and above), the increase in the cluster size will further increase the molecular weight.

Overall, despite subtle differences, the bituminous coals have similar carbon skeletal structures. However, the low-rank Monarch coal showed clear differences that were detrimental to its carbon fiber precursor production utilization. The smaller aromatic clusters with long aliphatic side chains rich in oxygen, coupled to a low content in carbon and a higher moisture level, would hinder economic utilization, although others have generated carbon fiber from this rank.[62]

3.4. Lattice Fringe Analyses from HRTEM Micrographs. Figure 2 shows HRTEM micrographs, and the lattice fringe micrographs are false-colored by length and false-colored by angle for the four coals in rank order from Monarch to Blue Gem. Observations are consistent with expectations based on coal science and rank. Low-rank coals have short fringes, with limited orientation and stacking.[18,19] The fringe length distributions change slightly with rank (and maceral influences,[18] although sharp edges are likely vitrinite particles) until low volatile bituminous to anthracite, where longer fringes are present with increasing frequency.[19]

At first glance, the fringe length distributions were similar for the Monarch, Herrin, and Springfield samples. When the data were consolidated for multiple micrographs, subtle differences in length distribution were more evident. More specifically, the low-rank Monarch coal had a distribution of shorter fringes, with the highest of the ranks examined here (Blue Gem) having slightly fewer benzene-sized fringes with a slightly greater contribution of naphthalene-sized structures. These observations are in agreement with the NMR data. Particularly for the Monarch coal, the high MW observed with NMR would relate to the presence of longer aliphatic chains with smaller aromatic cores. Additionally, following the established trend, the Herrin and Springfield coals had similar fringe distributions (Figure 2).

While naphthalene, anthracene/phenanthrene, and larger molecules can form mesophase during heating,[63] the presence of smaller molecules can interfere with the alignment and ordering of the molecules. For high-quality graphite-rich carbon fiber production from coal extracts, benzene and similar molecules must be removed (or combined to form

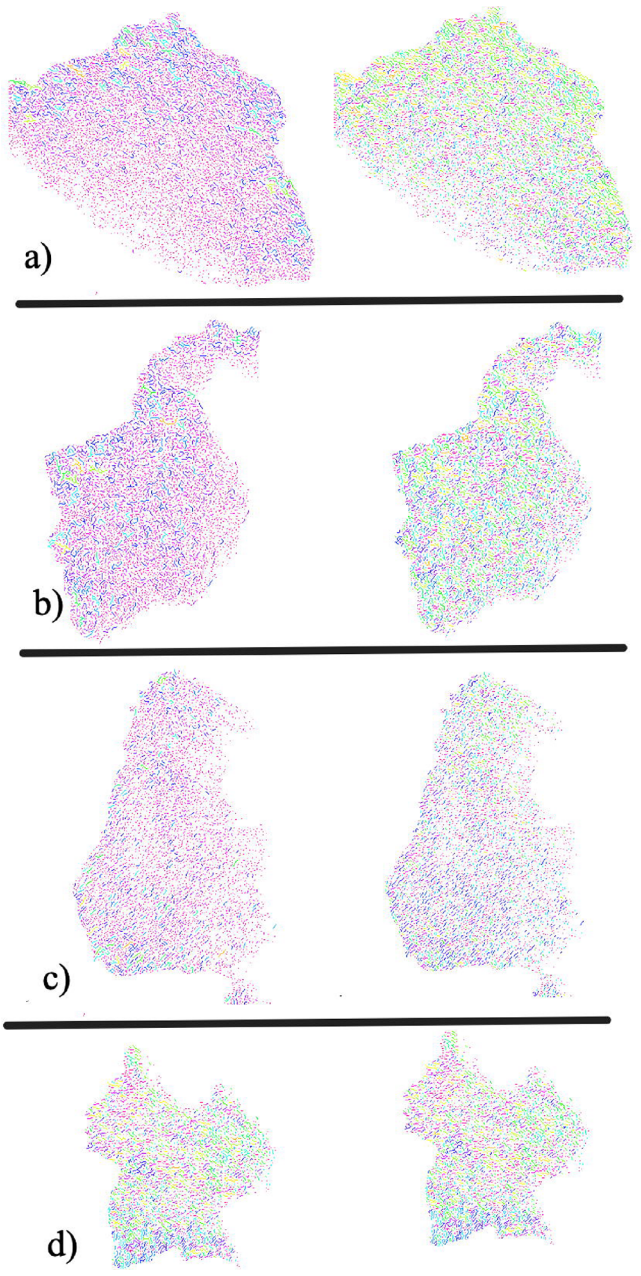

Figure 2. HRTEM micrographs of the regions of interest false-colored by fringe length (left-hand side) and by fringe angle (right-hand side) for (a) Monarch, (b) Herrin, (c) Springfield, and (d) Blue Gem.

larger PAH molecules). In agreement with the NMR data, the HRTEM data for the bituminous coals revealed the bituminous coals to be more suitable candidates for precursor production from a structural perspective with their more appropriately sized aromatic building blocks.[64]

The fringe length distribution is also displayed graphically in Figure 3. From the molecule assignments, the carbon fraction of bridgehead carbons (f_a^B) can be estimated and compared with ^{13}C NMR data. There is good agreement between the techniques for f_a^B for the bituminous coals (0.28 vs 0.25, 0.25 vs 0.24, and 0.28 vs 0.25 in rank order from Herrin to Blue Gem) for HRTEM and NMR, if the larger molecules (>3 × 3 rings) are removed. The limited presence of large PAH molecules is also supported by wet chemistry approaches for

https://doi.org/10.1021/acs.energyfuels.3c05200
Energy Fuels XXXX, XXX, XXX−XXX

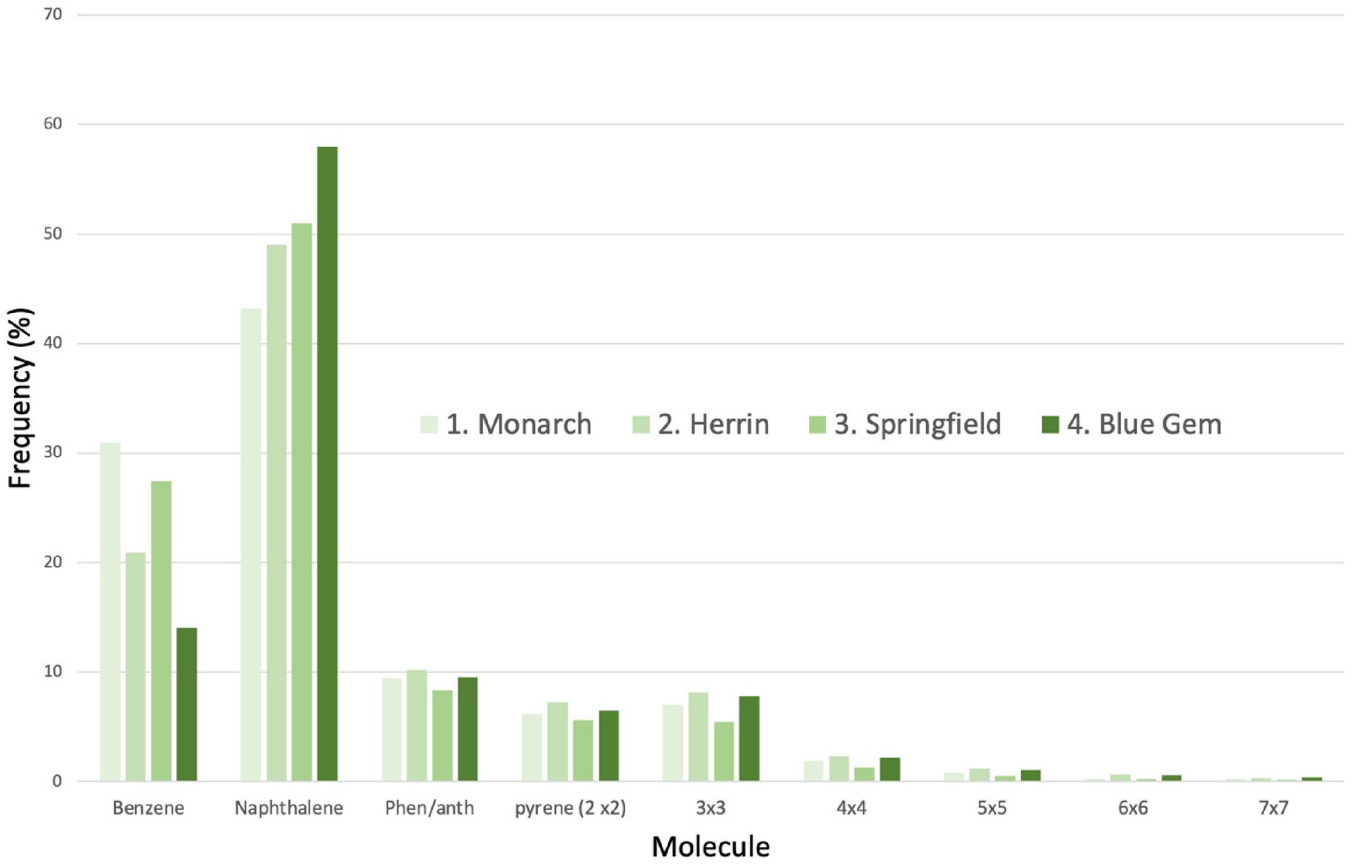

Figure 3. Fringe length distributions from multiple micrographs for each sample.

these ranks (limited contribution of coronene and larger structures observed as benzene hexacarboxylic acid following ruthenium ion-catalyzed oxidation (RICO) for bituminous ranks[65] but higher for anthracite).[32] Their presence in HRTEM micrographs could be due to apparently overlapping fringes or errors in the threshold selection step for binarization.

The agreement was poorer for the Monarch coal 0.26 vs 0.20 (HRTEM to NMR), keeping in mind that the micrographs had limited stacking and orientation degree (see the false-colored by angle (Figure 2) as expected for these ranks).[19] Regardless, the good agreement between the NMR and HRTEM results, at least for the bituminous coals, established a detailed carbon skeletal structure. In the following sections, chemistries and the complexities of the molecular structures will be discussed.

3.5. Molecular Weight Estimates with LDI. The organic matrix of coal is a highly complex mixture of small to very large molecules due to the countless chemical reactions occurring over the formation of the coalbed from a highly heterogeneous distribution of starting products.[34] Accordingly, various spectroscopic techniques need to be employed to assess the molecular size distributions and their chemical compositions and structures. To begin this section, first, the mass spectra of the raw coals obtained from the LDI-MS measurements at Penn State University are shown in Figure 4 in order of coal rank from Monarch (lowest) to Blue Gem (highest) using the mass-to-charge ratio (m/z) distributions.

The mass distributions obtained from the demineralized coals at ORNL's CNMS are presented in Figure 5.

Comparing Figures 4 and 5, the raw coals have peaks in the 500 to ~750 m/z range, while the second instrument (Bruker

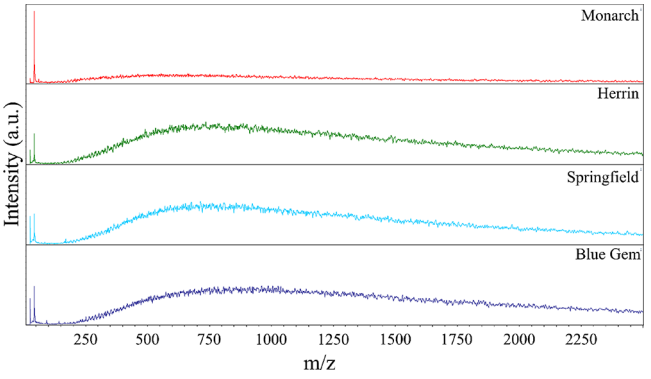

Figure 4. Laser desorption ionization mass spectra from raw coals Monarch, Herrin, Springfield, and Blue Gem from top to bottom, obtained at Penn State University.

Autoflex Speed MALDI-TOF) with demineralized samples (Figure 5) shows that three bituminous coals have an apparent bimodal mass distribution. The distributions in Figure 5 can be divided into low- and high-mass regions, with the low-mass peaks centered around 234, 348, 340, and 377 m/z for the Monarch, Herrin, Springfield, and Blue Gem coals, respectively. On the other hand, the higher mass peaks are centered around 1076, 958, and 988 m/z for the Herrin, Springfield, and Blue Gem coals. However, while small amounts of higher m/z peaks are observed for the Monarch coal, the higher molecular weight mode was much less intense than the other samples.

Overall, both approaches show similar profiles for the bituminous coals (Figures 4 and 5b–d) but with differences between techniques. The MALDI examination of Argonne

https://doi.org/10.1021/acs.energyfuels.3c05200
Energy Fuels XXXX, XXX, XXX−XXX

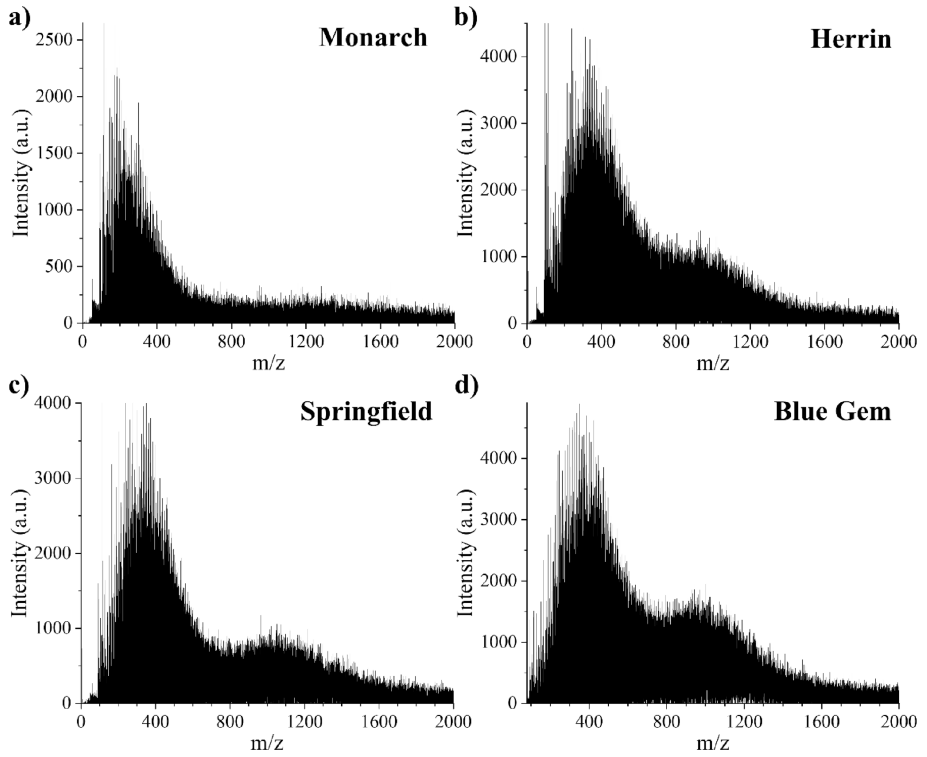

Figure 5. Laser desorption ionization mass spectra from demineralized coals: (a) Monarch, (b) Herrin, (c) Springfield, and (d) Blue Gem, obtained at ORNL.

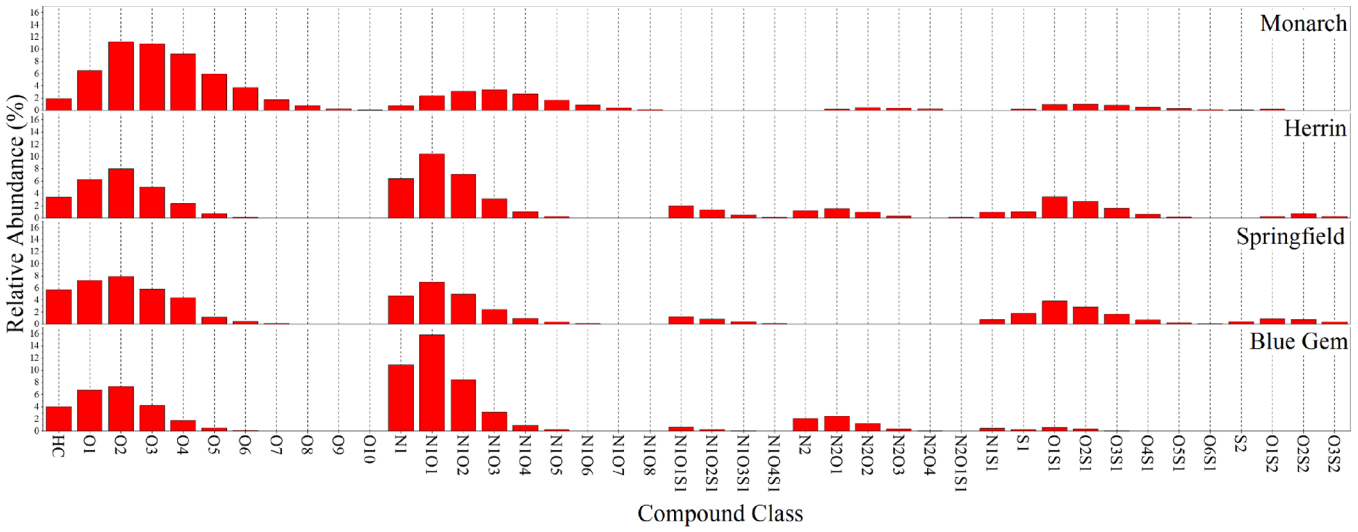

Figure 6. Distribution of the compound classes in the coal extracts for Monarch, Herrin, Springfield, and Blue Gem from top to bottom.

coals generally produced the classic single obvious peak with a long tail.[66] The coals of similarity to the coals explored in our carbon fiber work are Wyodak–Anderson (subB), Pittsburgh no. 8 (hvAb), and Upper Freeport (mvb), and these ranks had peaks centered ~400–500 Da as observed here (~400 Da). Dual peaks have also been observed for the Argonne Pittsburgh coal (400 and 2200 amu) using the MALDI approach.[67] It was reported that demineralization (specifically, acid treatment of the extract) did not significantly change the molecular weight profile of coal extracts (although the demineralization process was different).[68] Hence, acid-catalyzed condensation reactions appear to be unlikely. Carbon clusters can also be produced by low-energy laser desorption of benzo(e)pyrene.[69] Thus, there are considerable challenges with molecular weight distribution estimates.[70]

In their extensive study with a wide range of coal ranks, Herod et al.[27] reported that smaller amounts of high molecular masses had been found for low-rank coals with a systematic increase in the higher molecular weight species with increasing coal rank. This agrees with the results presented here, where the low-rank Monarch coal has molecular masses smaller than those of the high-rank bituminous coals. The Blue Gem coal (the highest rank explored here) contributes more to higher molecular weight species than the other bituminous coals. Also, when we focus on the low molecular weight distribution, the Blue Gem coal has a slightly higher molecular weight than

https://doi.org/10.1021/acs.energyfuels.3c05200
Energy Fuels XXXX, XXX, XXX−XXX

the others, with Monarch showing the lowest molecular weight, in accordance with general rank expectations.

3.6. Identification of Unique Molecules with FT-ICR MS. Each peak in an FT-ICR mass spectrum (see example in Figure S1, Supporting Information) corresponds to a unique compound (within at least 12,000 compounds detected here for a single coal); these data sets need to be convoluted into broader classifications to better discern the differences between these coal extracts. One such representation comes in the form of compound class distributions, where molecule classes are grouped together if they contain the desired heteroatoms. The distribution of pure hydrocarbons (HC) as well as heteroatom compounds (O_o, N_n, S_s, O_oS_s, N_nO_o, N_nS_s, and $N_nO_oS_s$) are presented in Figure 6 for the coal extracts as a function of their relative abundances. Here, as an example, the O_1 class are the molecules that contain one oxygen atom, the O_2 class contains two, and so on.

For the pure HC class, the relative abundances within all of the detected compounds remained relatively low at ~4−5% for the bituminous coals (the highest being in Springfield) and ~2% for the low-rank Monarch. The O_o class distributions were similar among the bituminous coals (with the O_2 class having the highest abundance). Springfield was slightly more complex (molecules with the oxygen content extending to O_7) compared with the other bituminous extracts. Monarch had a high abundance of the oxygen molecule classes extending to O_{10} with the highest abundances in O_2 and O_3 classes. This is to be expected from its low rank and higher oxygen content (Table S1). The N_1 and N_1O_o classes show similar types of distributions for the bituminous coal extracts, however, with greater overall significance for Blue Gem in accordance with its higher bulk N content based on ultimate analyses (Table S1). Also, the majority of the oxygen atoms bound in complex heteroatom groups (with two or more types of heteroatoms) are observed to be of N_1O_o type for Blue Gem. While the N_1O_1 type compounds have the highest abundance for the bituminous coal extracts, for Monarch, the highest relative abundance is N_1O_3 with the series extending to N_1O_8 with a more uniform distribution.

The first major discrepancy between the bituminous coal extracts occurs in the N_2 and N_2O_o classes, which are missing in the Springfield sample while being present in the others with subtle distribution differences. Interestingly, while the Monarch coal extract does not show N_2-type compounds, its oxides are present up to N_2O_4. The second major discrepancy among the bituminous coal extracts occurs in S_1, S_2, S_1O_o, and S_2O_o groups. Blue Gem having the lowest bulk sulfur content (Table S1), shows the least amount of sulfur-containing molecules with the S_2 variety completely absent. Springfield and Herrin, however, reveal similar distributions in agreement with their similar bulk sulfur contents. Yet, the Springfield coal extract has a higher concentration of S_2O_o-containing molecules. Monarch being exceptionally low in sulfur but high in oxygen showed relatively lower amounts of S_1 and O_oS_1-type components extending up to O_6S_1 with more limited S_2 and O_1S_2-type molecules. Finally, with increased molecular complexity (e.g., $N_1O_oS_1$) particularly, the Monarch coal extract did not show any detectable compounds.

While the compound class distributions are useful as a first approach to distinguish compositional differences, they do not contain detailed molecular information. This can be overcome by plotting the molecular compositions using isoabundance contoured plots of double-bond equivalents (DBE) vs C numbers, enabling visual representation of thousands of compounds in a single graphical form.[29,33,34,45] Here, the DBE number increases by one with the addition of either of the following to the structure: a double-bond, a ring, a keto, or a carboxylic group,[34] whereas the C number would increase linearly with each new C atom added to the structure.

3.6.1. Isoabundance Plots. The DBE-CN distributions from the pure hydrocarbon (HC) and single heteroatom (O_1, N_1, and S_1) classes are presented in Figure 7 for the coal extracts.

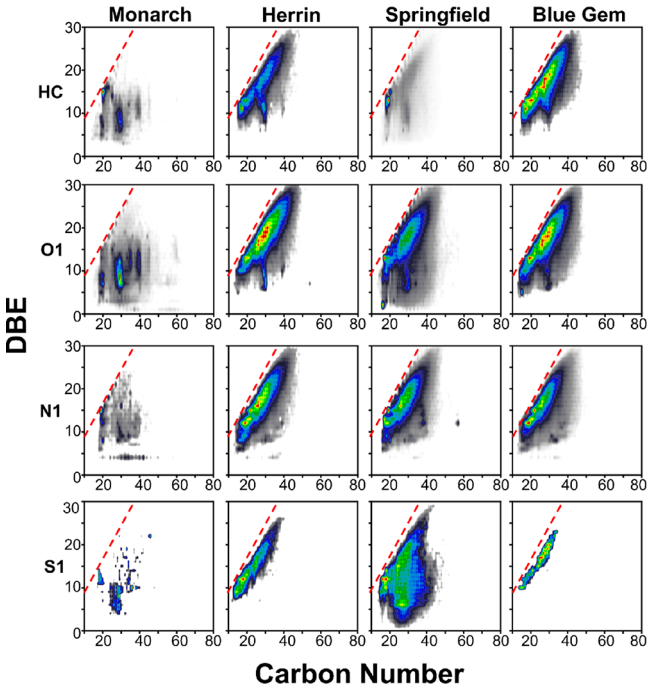

Figure 7. Isoabundance contour plots of the HC, O_1, N_1, and S_1 class distributions presented by using DBE-CN relations for the coal extracts for Monarch, Herrin, Springfield, and Blue Gem from left to right. Each plot is normalized to the highest signal abundance for each class.

Each point along the experimentally determined planar limits in DBE-CN plots corresponds to the beginning of each homologous series for the investigated molecule group, wherein each addition of a new point to a homologous series (i.e., CN+1) corresponds to the addition of one C atom to the alkyl side chains.[33] Within this context, particularly the presence of lower DBE, higher CN species points to the presence of aliphatic compounds,[29] wherein as the CN extends higher, it indicates the presence of long or multiple short alkyl chains attached to the aromatic core.[41]

When plotting the DBE-CN distributions, a DBE = 0.9C (slope) rule is obeyed for the maximum allowable PAH limit, which signifies a compositional boundary to exclude impossible or inaccessible chemical formulas.[71] This limit is indicated with a red dashed line. The planar limit slope also corresponds to the degree of structural condensation of the aromatic core (i.e., a higher slope indicates higher aromaticity).[72]

3.6.1.1. Pure Hydrocarbons (HC). The class HC (hydrocarbons with no heteroatoms) contains the most useful molecules for conversion processes;[33] however, its relative abundance remains limited to 4−5% for the bituminous coal

https://doi.org/10.1021/acs.energyfuels.3c05200
Energy Fuels XXXX, XXX, XXX−XXX

extracts and even less for the subbituminous Monarch coal extract as described in Section 3.4. The HC isoabundance plots in Figure 7 present similar profiles (with similar degrees of condensation) for the bituminous coal extracts with an important caveat for Springfield that shows a very strong concentration (i.e., hotspot) for the $C_{19}H_{14}$ molecule (with DBE = 13) that effectively skews the relative abundance values for the rest of the molecules. On the other hand, the Monarch coal extract mostly occupies the low DBE regime (low aromaticity) with higher H/C ratios (i.e., more saturated structures) in agreement with its low rank and the NMR results. Additionally, for the Springfield coal extract, HC molecules occupy the lower DBE (<10) zone with a large aliphatic spread in a CN range 15−45, suggesting a higher molecular complexity than Blue Gem and Herrin. This will be discussed in more detail later in this section.

Based on the slopes of the DBE-CN curves, possible structures had previously been calculated using simple models. Here, a slope of 0.25 corresponds to structures formed by adding saturated cyclic rings (naphtenic rings). The linear addition of aromatic rings would yield a slope of 0.75 (cata-condensation), whereas a serial nonlinear addition of aromatic rings (peri-condensation) would result in a slope of 1 (0.9 within the limits of FT-ICR data).[41,73] Following this, the slopes are calculated for the HC, O_1, N_1, and S_1 classes solely using the DBE-CN relation, irrespective of the relative abundance differences. The results are presented in Table 3.

Table 3. Planar Aromatic Limit Slopes for the HC, O_1, N_1, and S_1 Classes for the Coal Extracts

	coal			
class	Monarch	Herrin	Springfield	Blue Gem
HC	0.66	0.65	0.80	0.67
O_1	0.90	0.73	0.78	0.71
N_1	0.71	0.65	0.74	0.65
S_1		0.72	0.74	0.69

Between the bituminous coals examined, Blue Gem and Herrin showed similar slopes (i.e., similar degrees of condensation), whereas Springfield shows the highest degree of condensation among all. Interestingly for Monarch, the O_1 class distribution shows a slope of 0.90 (at the maximum PAH limit for FT-ICR), suggesting the presence of highly condensed core structures for this class (although this is not the expected observation) while also showing long alkyl chains.

Further examining the HC protonated ion data, multiple comparisons can be made between the studied coals, for example, the lowest and highest ranks (Monarch and Blue Gem) and the ranks that are very similar on average properties (Herrin and Springfield). Starting with the Monarch and Blue Gem coals, there were similar unique HC molecular compositions (485 vs 457, respectively) with a 60.2% overlap (i.e., molecules appearing in both coals). This overlap was very high in the C18 to C32 range (96.9%), with a poorer agreement in the lower (C14−18) and higher carbon numbers (C33−50).

The expectation for the Herrin and Springfield coals was for a high similarity, given the similarity in the other analytical data presented in the previous sections. Indeed, this was the case with a 99.1% overlap in composition when the Herrin coal was compared with the Springfield coal. However, there were differences in molecular complexity: 470 vs 765 unique HC molecules, with Springfield being much more complex. Thus, the comparison goes in the other direction: Springfield vs Herrin, was much lower at 60.7%. A comparison of the Springfield and Blue Gem was expected to have a lower overlap, given the slightly higher maturation of the Blue Gem coal, and this was indeed the case with an 80.9% overlap for Blue Gem vs Springfield and 42.8% if the comparison order was reversed. While a molecule-by-molecule comparison cannot be presented here, given the vast amount of data, the data set can be condensed into a table of C and H numbers. This is presented in Table S1 of the Supporting Information.

While identical compositions do not necessarily imply the same structures (particularly in larger molecules where the number of structural isomers is high), in the case of the bituminous coals formed in the same basin at a similar time and with similar coalification experiences, some of these structures are likely very similar. Here, 21740, 16931, 30190, and 12982 unique compositions were identified for the Monarch, Herrin, Springfield, and Blue Gem coals, respectively. A similar overlap comparison was performed by using all of the identified molecules (i.e., including heteroatoms) to explore the greater diversity between the coals. This approach provides some insight into the structural similarities between ranks. In this context, the similarity between Blue Gem and Herrin for all compositions was 84.7% (i.e., Blue Gem contained 84.7% of the unique molecules Herrin had) but only 45.1% for Herrin vs Blue Gem. Next, the overlap was 87.6% for Blue Gem vs Springfield, while Springfield vs Blue Gem was 53.7%. Overall, similar to the results for pure HC molecules, there is considerable overlap between the bituminous coals, albeit with Springfield demonstrating a much higher complexity than the others, despite being very similar to the Herrin coal in many average (nondistribution) parameters, as seen in previous sections (e.g., FTIR and NMR). This can be traced back to the subtle differences in the botanical inputs and the amount and the type of the macerals and in the responses of these macerals to diagenesis and metamorphism.[74]

The presence of heteroatoms is undesirable in the conversion product (e.g., carbon precursor) and accordingly necessitates further processing of the raw coal feedstock by means of deoxidation, denitrogenation, and desulfurization. While most of these could occur during an upgrading process like hydroconversion, eliminating all heteroatoms may be impossible. In addition to the number of heteroatoms, it is equally important (if not more important) to know how they are incorporated into the molecular structure. For example, a candidate with lower heteroatoms and easily breakable bonds represents the best-case scenario. The following sections investigate the various heteroatom moieties in more detail.

3.6.1.2. Oxygen-Containing Functionalities. The oxygen atoms in the precursor structure can lead to oxidation reactions during further processing operations to the pitch and carbon fiber. The cross-linking caused by oxygen molecules inhibits melting and flow, effectively blocking the pitch to fiber processing. The ultimate analysis and the other spectroscopic techniques employed here revealed the Monarch coal to have the highest amount of oxygen, as is typical of low-rank subbituminous coals. Furthermore, the oxygen-containing molecules were found in more complex structures with single heteroatom compounds detected up to O_{10} (Figure 6). The O_1 class isoabundance distribution revealed the Monarch coal molecules to have the most condensed core structure (Table

https://doi.org/10.1021/acs.energyfuels.3c05200
Energy Fuels XXXX, XXX, XXX−XXX

3) and the longest aliphatic side chains with carbon number (CN) extending up to 65, in agreement with the NMR results (Table 2). Accordingly, most of the detected molecules were found to occupy lower DBE regions. Because of these, Monarch coal is the least favorable candidate, based on expected carbon yield, for pitch-based carbon fiber production within the examined coal set.

Like the pure HC distributions, the bituminous coals present a similar O_1 class distribution with relatively short side chains. However, the Springfield coal extract can again be observed to extend further into the lower DBE and higher H/C groups of molecules (Figure 7). It should also be emphasized that while the molecular cores contribute the most to chemical reactivity and physical properties, the oxygen functional groups in side chains would also need to be removed before fiber spinning.

3.6.1.3. Nitrogen Functionalities. Expectations are that the N-class species will primarily reside in either 5-membered (pyrrolic) or 6-membered rings (pyridinic).[39,75] According to Purcell et al.,[75] N-containing aromatics under APPI ionization form radical cations if N is within a pyrrolic moiety and protonated molecules if the N form is pyridinic. Thus, while the N_1 class likely corresponds to pyridinic nitrogen, the N_2 and N_3 classes can be in pyrrolic or pyridinic.[29] In agreement with this, the N_1 class molecules detected in our coal extracts were mostly of a protonated moiety, that is, pyridinic. However, based on previous XPS work, pyrrolic N is reported to be the dominant form in coal.[76] The XPS results from our coals support this with a higher presence of pyrrolic N at a more macrolevel (compared to FT-ICR) with 65, 68, and 76% dominance in the Blue Gem, Springfield, and Herrin coals, respectively. This could be related to selective extraction of certain species during solvent extraction for the FT-ICR measurements.

Acquired XPS spectra from the Herrin coal are presented in Figure 8 to show the N 1s peaks and the position of the

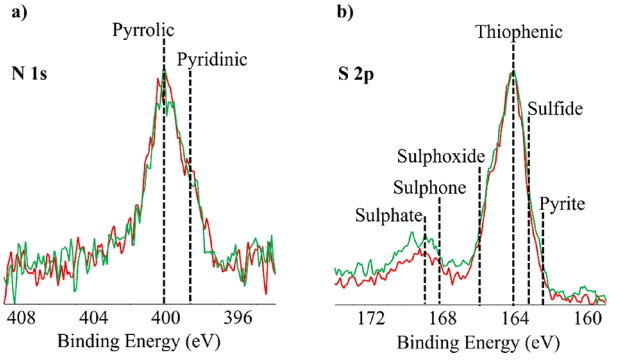

Figure 8. (a) XPS N 1s and (b) S 2p bands of the Herrin coal presented with the individual peak locations of reference compounds. The red and green patterns correspond to data from two separate sampling locations.

component peaks. The Monarch coal is excluded from the XPS studies as it is deemed less suitable for further processing due to its very high oxygen content deeply incorporated into its molecular network.

It has been reported that N atoms in coals are generally fused in aromatic rings.[39] The isoabundance plots in Figure 7 support this argument, at least for the bituminous coals, which show a similar distribution. Small variations are present where the Blue Gem coal shows a slightly tighter distribution (while being mostly identical to Herrin), whereas Springfield extends to slightly more aromatic (higher DBE) molecules. Conversely, Monarch shows clear differences where the aromatic cores are smaller overall with longer aliphatic side chains (low DBE at high CN). From a denitrogenation perspective, Blue Gem coal with its highest bulk N content (Table S1) that carried over to the relative abundance distribution of the molecular classes (Figure 6) with a heavy concentration in the aromatic core structure would be the most challenging. Accordingly, even with added hydroconversion, some of the N-containing molecules are expected to be retained in the pitch. While the effects of N on further pitch-processing are unknown, the N-molecules are not expected to make it into the final fiber product as they leave the structure during the gasification process.

3.6.1.4. Sulfur Functionalities. Sulfur in coal can exist as either thiophenic functionalities as part of the aromatic cores or in alkyl side chains as sulfides.[33,40,41] Alkyl sulfides are more likely to form H_2S during high-temperature conversion processes such as graphitization, while thiophenic functionalities are more resistant and more likely to remain in the residual pitch during pyrolysis.[33] Aside from environmental concerns (e.g., the release of H_2S), sulfur that persists in the pitch can further lead to premature cross-linking during the conversion processes. Accordingly, of all the heteroatoms present, S is the most undesirable.

Based on previous FT-ICR MS data, S_1 molecular compounds with DBE values <4−6 are reported more likely to be sulfides, while those with DBE > 4−6 are likely to be of thiophenic nature.[33,40] Based on this, the S_1 compounds observed in the Blue Gem and Herrin coal extracts are expected almost exclusively to be thiophenic (Figure 7). The Springfield, however, shows a significantly different distribution with a major presence of sulfides. Finally, the Monarch, being exceptionally low in bulk sulfur (Table S1), did not show many detectable S_1 compounds in its extract, with most of the detected compounds being sulfides, as seen in Figure 7.

The XPS bands of S 2p are harder to deconvolute compared to N 1s and can be affected by sulfur in inorganic compounds, such as pyrite. Moreover, a significant number of potential molecules can contribute to this spectra, therefore, making it prone to potential fitting errors. Previously, the XPS S 2p spectra were fitted with multiple compounds, namely, pyrite (162.5 eV), sulfides (163.3 eV), thiophenes (164.1 eV), sulfoxides (166.0 eV), sulphones (168.2 eV), and sulfonic acids/sulfates (169.0 eV)[77] (see locations in Figure 8). For this work, the XPS data was used to qualitatively determine the dominant form of the sulfur compound, revealing a majority of thiophenic variety for the bituminous coals examined (example pattern in Figure 8).

The isoabundance plots in Figure 7 show a very narrow (almost linear) S_1 distribution for the Blue Gem coal extract suggesting these compounds to be composed of condensed aromatic units without large alkyl chains.[33,45] The Herrin coal extract shows a similar type of distribution with slightly longer side chains than Blue Gem. Regardless, the sulfur atoms are heavily incorporated into the aromatic cores of these two coals and can be expected to persist in the pitches obtained from these coals. The Springfield coal extract, on the other hand, shows a significantly different S_1 molecular distribution that extends to higher and lower aromaticities (based on DBE distributions) and contains significantly longer side chains. While the long aliphatic chains can be separated from the

https://doi.org/10.1021/acs.energyfuels.3c05200
Energy Fuels XXXX, XXX, XXX−XXX

aromatic cores via methods like thermal cracking,[33] the aromatic sulfur would likely persist in the pitch (at least partially) similar to the other bituminous coals. A molecular investigation of the pitches produced from these coal precursors would be beneficial in understanding the beneficiation processes and serve as the next step in compositional mapping toward carbon fiber production.

3.6.1.5. Complex Heteroatom Groups. Compound classes with more unique heteroatoms are considered to be more complex molecules. Based on the total abundances, 48, 44, 54, and 27% of the identified molecules from Blue Gem, Springfield, Herrin, and Monarch are complex heteroatoms (containing at least two heteroatom types). However, it must be stated that selective ionization of the APPI technique makes this comparison highly qualitative, and the relatively small differences between the bituminous coals should not be overanalyzed. Still, the difference between bituminous and subbituminous coals is appreciable and follows the expected behavior of low-rank coal.

Isoabundance distribution plots for the N_1O_1, N_1S_1, and O_1S_1 heteroatom groups are presented in Figure 9.

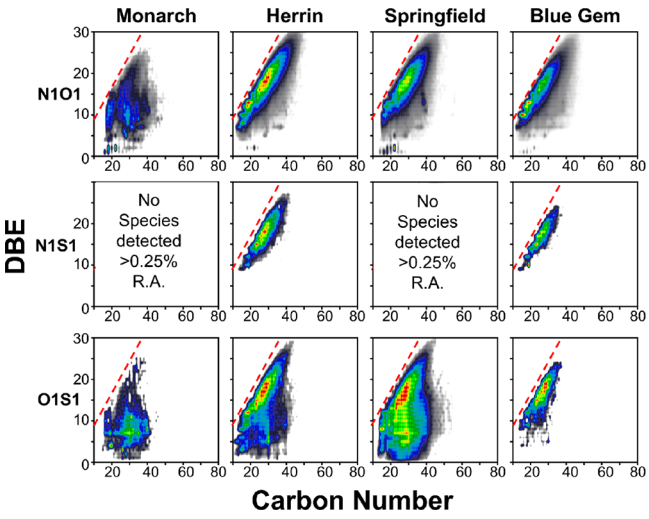

Figure 9. Isoabundance contour plots of the N_1O_1, N_1S_1, and O_1S_1 class distributions presented using DBE-Carbon number relations for all of the coal extracts for Monarch, Herrin, Springfield, and Blue Gem coals from left to right. Each plot is normalized to the highest signal abundance for each class.

Starting with the N_1O_1 class, relatively similar distributions are observed for the bituminous coals, where the level of alkylation increased from Blue Gem to Herrin and Springfield. Interestingly, a small cluster of molecules with very small aromatic cores (DBE of 1−3) is also observed for all the coal extracts. A more aliphatic structure with longer side chains is observed for Monarch compared to the others, as would be expected from previous sections. The N_1S_1 class, however, is only observed in the Blue Gem and Herrin coal extracts with mostly condensed structures and limited alkylation.

For the O_1S_1 group, while the Springfield coal extract showed a somewhat similar distribution to that of its S_1 group with high levels of alkylation, the major differences were observed for the Herrin coal extract, followed by the Blue Gem. It was previously reported that common structural moieties (with two different heteroatoms) containing sulfur are mostly thiophenic, with varying amounts of functional groups containing the secondary element, such as oxygen, in this case.[34] Adding oxygen functional groups could help explain the increased alkylation in the Blue Gem and particularly the Herrin coal extracts, where this effect is most pronounced. Compared to pure S_1, the increased alkylation is also visible in the Monarch coal extract. The same reasoning could also help explain the lack of significant alkylation in the N_1S_1 group, as N is mostly fused in the aromatic cores.[39]

Finally, the Monarch coal extract showed noticeably increased aromaticity for oxygen-containing complex heteroatoms compared to that of single heteroatom groups. This was also observed for other complex heteroatom groups, including N_nO_o and O_oS_s types (not shown here). This is an expected outcome based on statistics wherein the bigger the molecule, the higher the odds of finding several heteroatoms in it.

As part of process development, following hydroconversion and pitch production, the samples must be remeasured to determine whether the heteroatom content has been reduced and if the complex heteroatoms have been broken down into simpler ones.

Overall, based on the extensive characterization work (previous[6,7] and current), the subbituminous Monarch and, by extension, low-rank coals are a less suitable raw feedstock for carbon fiber precursors, at least cost-competitively. The bituminous coals showed potential for further investigation, with the highly volatile A bituminous Blue Gem (based on molecular data) having a slight edge over the others. Such behavior can also be extrapolated to higher-rank coals. More importantly, with the experiment-driven molecular models, processing routes can be simulated repeatedly until the best utilization approach is obtained.

4. SUMMARY AND CONCLUSIONS

This work presents a detailed molecular characterization of three bituminous (Herrin, Springfield, and Blue Gem) and one subbituminous (Monarch) coals, to help assess their suitability as raw feedstock materials for carbon fiber precursor production.

Fourier transform infrared (FTIR) spectroscopy revealed the presence of similar spectra across all coal samples, with only minor unique features. Notably, a distinct peak around 1700 cm^{-1} was seen in the Monarch coal, which could represent specific heteroatoms in this coal, potentially concealed within the broader features of the other coal samples.

Between the bituminous coals, their carbon skeletal structures were overall very similar, with Blue Gem showing small differences in accordance with its relatively higher rank, as revealed by solid-state ^{13}C nuclear magnetic resonance (NMR) spectroscopy. The subbituminous Monarch coal showed major differences wherein it comprised of smaller aromatic clusters with longer aliphatic chains and higher oxygen functionalities. These long aliphatic chains also resulted in the highest average molecular cluster weight in Monarch. On the other hand, the increased oxygen loss through maturation led to decreased aliphatic branching and the lowest average cluster weight in Blue Gem. Further, the least cross-linked structure was found in Monarch, while the most was in Blue Gem.

In line with the NMR results, high-resolution transmission electron microscopy (HRTEM) revealed the Monarch coal to have a distribution of shorter fringes (i.e., smaller molecules) while the higher rank bituminous coals consisted of benzene-,

https://doi.org/10.1021/acs.energyfuels.3c05200
Energy Fuels XXXX, XXX, XXX−XXX

naphthalene-, and anthracene/phenanthrene-sized fringes, which can form mesophase during heating. Larger PAH molecules were deemed necessary for high-quality graphite-rich carbon fiber production from coal extracts, making the bituminous coals more suitable for precursor production from a structural perspective.

Laser desorption ionization (LDI) mass spectroscopy (MS) measurements revealed the bituminous coals to have similar mass distributions. The high mass region was very weak in the low-rank Monarch coal, where higher molecular masses are related to increased molecular complexity. By the same reasoning, the highest rank coal Blue Gem had a larger contribution of higher molecular weight species to its overall mass distribution.

Fourier transform ion cyclotron resonance (FT-ICR) MS has revealed that only ∼4−5% of the detected species were of the pure HC class for the bituminous coals, which reduced further to 2% for Monarch. The remaining molecules were always associated with heteroatoms, where the O_o class was the most abundant of single heteroatom-containing species. While the O_o class distributions were similar between bituminous coals, for the Monarch coal, oxygen was found to be a key structural component extending up to the level of the O_{10}, with potentially highly condensed core structures. This was combined with the longest aliphatic side chains in this lower-rank coal. With such a high level of incorporation of the oxygen atoms into its organic structure, the Monarch coal was the least fit for further processing.

The sulfur atoms were found to be highly incorporated into the aromatic structure when present, even in small quantities (e.g., Blue Gem). Its presence was more pronounced in the Springfield coal, with heavy aliphatic branching among the bituminous coals. Since sulfur is the most unwanted heteroatom for carbon fiber processing (premature cross-linking), its presence must be monitored in the pitches derived from these coals and mitigation strategies developed. The heterogeneous nature of coals makes this a challenging process as established by this pilot study.

The challenge can yet be overcome, and vast coal resources can be processed into high-value-added industrial products. However, this requires an initial research investment in two major areas: (1) the formation of comprehensive property databases from multiple length scales and (2) generation of accurate molecular models. Carbon fiber precursor development is just one proposition, and as progress is achieved in these areas, alternative value-added use cases for this vast natural resource will be developed. Our current efforts have yielded successful production of carbon fibers from coal precursors, and results are currently being prepared for dissemination.

■ ASSOCIATED CONTENT

Supporting Information

The Supporting Information is available free of charge at https://pubs.acs.org/doi/10.1021/acs.energyfuels.3c05200.

Additional results for coal petrology and FT-ICR MS (PDF)

■ AUTHOR INFORMATION

Corresponding Author

Ercan Cakmak − *Materials Science and Technology Division, Oak Ridge National Laboratory, Oak Ridge, Tennessee 37831, United States;* orcid.org/0000-0001-7272-4815; Phone: (865) 574-6538; Email: cakmake@ornl.gov

Authors

Jonathan P. Mathews − *John and Willie Leone Family Department of Energy and Mineral Engineering, & The EMS Energy Institute, Pennsylvania State University, State College, Pennsylvania 16801, United States*

Sungsool Wi − *National High Magnetic Field Laboratory, Florida State University, Tallahassee, Florida 32310, United States*

Matthew R. Ryder − *Materials Science and Technology Division, Oak Ridge National Laboratory, Oak Ridge, Tennessee 37831, United States;* orcid.org/0000-0002-1363-8148

Martha Chacón-Patiño − *National High Magnetic Field Laboratory, Florida State University, Tallahassee, Florida 32310, United States;* orcid.org/0000-0002-7273-5343

Amy M. McKenna − *National High Magnetic Field Laboratory, Florida State University, Tallahassee, Florida 32310, United States; Department of Soil and Crop Sciences, Colorado State University, Fort Collins, Colorado 80521, United States;* orcid.org/0000-0001-7213-521X

Frederic Vautard − *Chemical Sciences Division, Oak Ridge National Laboratory, Oak Ridge, Tennessee 37831, United States*

Mark Arnould − *Center for Nanophase Materials Sciences, Oak Ridge National Laboratory, Oak Ridge, Tennessee 37831, United States*

Harry Meyer, III − *Chemical Sciences Division, Oak Ridge National Laboratory, Oak Ridge, Tennessee 37831, United States*

Edgar Lara-Curzio − *Energy Science and Technology Directorate, Oak Ridge National Laboratory, Oak Ridge, Tennessee 37831, United States*

Complete contact information is available at: https://pubs.acs.org/10.1021/acs.energyfuels.3c05200

Notes

The authors declare no competing financial interest.

■ ACKNOWLEDGMENTS

This research work was sponsored by the U.S. Department of Energy Fossil Energy and Carbon Management Program, Advanced Coal Processing Program, C4WARD project (FEAA155). A portion of this work was performed at the National High Magnetic Field Laboratory ICR and NMR User Facilities, which are supported by the National Science Foundation Division of Chemistry and Division of Materials Research through DMR-1644779, DMR-2128556, and the State of Florida. The HRTEM micrographs were obtained by

Akshay Gharpure at Penn State. The LDIMS data at PSU was generated by Tatiana Laremore. The authors acknowledge the use of the Penn State Materials Characterization Lab for the HRTEM and LDiMS facilities. Laser desorption ionization analysis was conducted at the Center for Nanophase Materials Sciences at ORNL, which is a DOE Office of Science User Facility.

REFERENCES

(1) Milici, R. C. Coal-to-liquids: potential impact on US coal reserves. *Natural Resources Research* **2009**, *18* (2), 85−94.
(2) Energy Information Agency. *Annual Coal Report 2021*; **2022**. https://www.eia.gov/coal/annual/.
(3) Reid, I. *Advances in-Non-Energy products from Coal*; IEA Clean Coal Centre, 2021. National Coal Council. *Coal in the New Carbon Age*. National Coal Council, 2019. https://www.nationalcoalcouncil.org (accessed.
(4) Azami, K.; Yamamoto, S.; Sanada, Y. Carbonization behavior of petroleum pitch—In situ high-temperature 13C-NMR measurements. *Carbon* **1993**, *31* (4), 611−615.
(5) Annamraju, A.; Jung, G. S.; Bhagia, S.; Damron, J. T.; Ryder, M. R.; Arnould, M. A.; Cakmak, E.; Vautard, F.; Paul, R. M.; Irle, S. On the role of methyl groups in the molecular architectures of mesophase pitches. *Fuel* **2024**, *357*, No. 129976.
(6) Cakmak, E.; Annamraju, A.; Mathews, J. P.; He, L.; Gallego, N.; Lara-Curzio, E. Characterization of Porosity and Pore Accessibility of Vitrinite-Rich Bituminous and Subbituminous Coals by Small-Angle Neutron Scattering, Mercury Intrusion Porosimetry, and Low-Pressure N2 Adsorption. *Energy Fuels* **2022**, 191 DOI: 10.1021/acs.energyfuels.2c02814.
(7) Cakmak, E.; Hower, J. C.; Mathews, J. P.; Weisenberger, M. C.; Kaplan, R.; Lacy, J.; Zhang, Y.; Lara-Curzio, E. Microstructural diversity and digestion yields of select bituminous and subbituminous coals as raw material candidates for carbon fiber precursor production. *Fuel* **2023**, *348*, No. 128545.
(8) Yoo, P.; Jung, G. S.; Ryder, M. R.; Vautard, F.; Cakmak, E.; Wi, S.; Weisenberger, M. C.; Lara-Curzio, E.; Mathews, J. P.; Irle, S. Large-scale atomistic model construction of subbituminous and bituminous coals for solvent extraction simulations with reactive molecular dynamics. *Carbon* **2024**, *222*, No. 118939.
(9) Ibarra, J.; Munoz, E.; Moliner, R. FTIR study of the evolution of coal structure during the coalification process. *Org. Geochem.* **1996**, *24* (6−7), 725−735.
(10) Wang, S.; Tang, Y.; Schobert, H. H.; Guo, Y. n.; Su, Y. FTIR and 13C NMR investigation of coal component of late Permian coals from southern China. *Energy Fuels* **2011**, *25* (12), 5672−5677.
(11) Ping, A.; Xia, W.; Peng, Y.; Xie, G. Construction of bituminous coal vitrinite and inertinite molecular assisted by 13C NMR, FTIR and XPS. *J. Mol. Struct.* **2020**, *1222*, No. 128959.
(12) Okolo, G. N.; Neomagus, H. W.; Everson, R. C.; Roberts, M. J.; Bunt, J. R.; Sakurovs, R.; Mathews, J. P. Chemical−structural properties of South African bituminous coals: Insights from wide angle XRD−carbon fraction analysis, ATR−FTIR, solid state 13C NMR, and HRTEM techniques. *Fuel* **2015**, *158*, 779−792.
(13) Solum, M. S.; Pugmire, R. J.; Grant, D. M. Carbon-13 solid-state NMR of Argonne-premium coals. *Energy Fuels* **1989**, *3* (2), 187−193.
(14) Fletcher, T. H.; Kerstein, A. R.; Pugmire, R. J.; Solum, M. S.; Grant, D. M. Chemical percolation model for devolatilization. 3. Direct use of carbon-13 NMR data to predict effects of coal type. *Energy Fuels* **1992**, *6* (4), 414−431. Chen, Y.; Lee, S.; Tahmasebi, A.; Bai, J.; Mahoney, M.; Yu, J. A review of the state-of-the-art research on carbon structure evolution during the coking process: from plastic layer chemistry to 3D carbon structure establishment. *Fuel* **2020**, *271*, No. 117657.
(15) Wang, C.; Zeng, F. Molecular Structure Characterization of CS2−NMP Extract and Residue for Malan Bituminous Coal via Solid-State 13C NMR, FTIR, XPS, XRD, and CAMD Techniques. *Energy Fuels* **2020**, *34* (10), 12142−12157.
(16) Solum, M. S.; Sarofim, A. F.; Pugmire, R. J.; Fletcher, T. H.; Zhang, H. 13C NMR analysis of soot produced from model compounds and a coal. *Energy Fuels* **2001**, *15* (4), 961−971.
(17) Rouzaud, J. N.; Guechchati, N.; Kister, J.; Conard, J. Structural characterization of coalification - example of Gironville borehole. *B Soc. Geol Fr* **1991**, *162* (2), 201−209. Sharma, A.; Kyotani, T.; Tomita, A. Quantitative evaluation of structural transformations in raw coals on heat-treatment using HRTEM technique. *Fuel* **2001**, *80*, 1467−1473.
(18) Sharma, A.; Kyotani, T.; Tomita, A. Direct observation of raw coals in lattice fringe mode using high-resolution transmission electron microscopy. *Energy Fuels* **2000**, *14*, 1219−1225.
(19) Mathews, J. P.; Sharma, A. The structural alignment of coals and the analogous case of Argonne Upper Freeport. *Fuel* **2012**, *95*, 19−24.
(20) Sharma, A.; Kyotani, T.; Tomita, A. Comparison of structural parameters of PF carbon from XRD and HRTEM techniques. *Carbon* **2000**, *38* (14), 1977−1984. Wang, C.; Huddle, T.; Lester, E. H.; Mathews, J. P. Quantifying curvature in HRTEM lattice fringe micrographs of coals. *Energy Fuels* **2016**, *30* (4), 2694−2704.
(21) Wang, C.; Watson, J. K.; Louw, E.; Mathews, J. P. A construction strategy for atomistic models of coal chars capturing stacking diversity and pore size distribution. *Energy Fuels* **2015**, *29* (8), 4814−4826.
(22) Van Niekerk, D.; Mathews, J. P. Molecular representations of vitrinite-rich and interinite-rich Permian aged South African coals. *Fuel* **2010**, *89* (1), 73−82.
(23) Fernandez-Alos, V.; Watson, J. K.; vander Wal, R.; Mathews, J. P. Soot and char molecular representations generated directly from HRTEM lattice fringe images using Fringe3D. *Combust. Flame* **2011**, *158* (9), 1807−1813. Leyssale, J. M.; Farbos, B.; Da Costa, J. P.; Weisbecker, P.; Chollon, G.; Vignoles, G. L. Analysis and molecular modeling of pyrolytic carbons nanotextures. In *High Temperature Ceramic matrix Composites 8: Ceramic Transactions*, Zhang, L., Jiang, D., Eds.; Vol. *248*; Wiley, 2014; pp 45−53.
(24) Narkiewicz, M. R.; Mathews, J. P. Improved low-volatile bituminous coal representation: incorporating the molecular weight distribution. *Energy Fuels* **2008**, *22* (5), 3104−3111. Castro-Marcano, F.; Lobodin, V. V.; Rodgers, R. P.; McKenna, A. M.; Marshall, A. G.; Mathews, J. P. A molecular model for the Illinois no. 6 Argonne Premium coal: moving towards capturing the continuum structure. *Fuel* **2012**, *95*, 35−49. Castro-Marcano, F.; Winans, R. E.; Chupas, P.; Chapman, K.; Calo, J. M.; Watson, J. K.; Mathews, J. P. Fine structure evaluation of the pair distribution function with molecular models of the Argonne Premium coals. *Energy Fuels* **2012**, *26*, 4336−4345. Huang, Y.; Cannon, F. S.; Guo, J.; Watson, J. K.; Mathews, J. P. Atomistic modeling insight into the structure of lignite-based activated carbon, and behavior of benzene sorption. *Rsc Adv.* **2016**, *6* (61), 56623−56637. Louw, E.; Mitchell, G. D.; Winans, R. E.; Mathews, J. P. Constitution of drop-tube generated coal chars from vitrinite-rich and inertinite-rich south African coals. *Energy Fuels* **2016**, *30*, 112−120. Wang, X.; Zhu, Y.; Chen, S.; Dai, X.; Xu, Q.; Song, Y.; Mathews, J. P. Molecular structure evaluation and image-guided atomistic representation of marine kerogen from Longmaxi Shale. *Energy Fuels* **2021**, *35* (9), 7981−7992. Zhang, Y.; Hu, S.; Zhong, Q.; Zhuo, J.; Mathews, J. P. A large-scale molecular model of Fenghuangshan anthracite coal. *Fuel* **2021**, *295*. DOI: 120616.
(25) Mathews, J. P.; Ferdandez-Alos, V.; Jones, D. A.; Schobert, H. H. Determining the molecular weight distribution of Pocahontas No. 3 low-volatile bituminous coal utilizing HRTEM and laser desorption ionization mass spectra data. *Fuel* **2010**, *89* (7), 1461−1469.
(26) Narkiewicz, M. R.; Mathews, J. P. Improved low-volatile bituminous coal representation: incorporating the molecular-weight distribution. *Energy Fuels* **2008**, *22* (5), 3104−3111.
(27) Herod, A. A.; Li, C. Z.; Parker, J. E.; John, P.; Johnson, C. A.; Smith, G. P.; Humphrey, P.; Chapman, J. R.; Kandiyoti, R.; Games, D. Characterization of coal by matrix-assisted laser desorption ionization

https://doi.org/10.1021/acs.energyfuels.3c05200
Energy Fuels XXXX, XXX, XXX−XXX

mass spectrometry. I. The Argonne coal samples. *Rapid Commun. Mass Spectrom.* **1994**, *8* (10), 808−814.
(28) John, P.; Johnson, C. A.; Parker, J. E.; Smith, G. P.; Herod, A. A.; Li, C.-Z.; Humphrey, P.; Chapman, J. R.; Kandiyoti, R. Molecular masses up to 270 000 u in coal and coal-derived products by matrix assisted laser desorption ionization mass spectrometry (MALDI-ms). *Fuel* **1994**, *73* (10), 1606−1616. Miura, K.; Shimada, M.; Mae, K.; Sock, H. Y. Extraction of coal below 350 C in flowing non-polar solvent. *Fuel* **2001**, *80* (11), 1573−1582.
(29) McKenna, A. M.; Chacón-Patiño, M. L.; Chen, H.; Blakney, G. T.; Mentink-Vigier, F.; Young, R. B.; Ippolito, J. A.; Borch, T. Expanding the Analytical Window for Biochar Speciation: Molecular Comparison of Solvent Extraction and Water-Soluble Fractions of Biochar by FT-ICR Mass Spectrometry. *Anal. Chem.* **2021**, *93* (46), 15365−15372.
(30) Roth, H. K.; Borch, T.; Young, R. B.; Bahureksa, W.; Blakney, G. T.; Nelson, A. R.; Wilkins, M. J.; McKenna, A. M. Enhanced Speciation of Pyrogenic Organic Matter from Wildfires Enabled by 21 T FT-ICR Mass Spectrometry. *Anal. Chem.* **2022**, *94* (6), 2973−2980. Bahureksa, W.; Borch, T.; Young, R. B.; Weisbrod, C. R.; Blakney, G. T.; McKenna, A. M. Improved Dynamic Range, Resolving Power, and Sensitivity Achievable with FT-ICR Mass Spectrometry at 21 T Reveals the Hidden Complexity of Natural Organic Matter. *Anal. Chem.* **2022**, *94* (32), 11382−11389.
(31) Wu, Z.; Jernström, S.; Hughey, C. A.; Rodgers, R. P.; Marshall, A. G. Resolution of 10 000 compositionally distinct components in polar coal extracts by negative-ion electrospray ionization Fourier transform ion cyclotron resonance mass spectrometry. *Energy Fuels* **2003**, *17* (4), 946−953.
(32) Wang, Y.-G.; Wei, X.-Y.; Xie, R.-L.; Liu, F.-J.; Li, P.; Zong, Z.-M. Structural characterization of typical organic species in Jincheng No. 15 anthracite. *Energy Fuels* **2015**, *29* (2), 595−601.
(33) Chacón-Patiño, M. L.; Blanco-Tirado, C.; Orrego-Ruiz, J. A.; Gómez-Escudero, A.; Combariza, M. Y. Tracing the compositional changes of asphaltenes after hydroconversion and thermal cracking processes by high-resolution mass spectrometry. *Energy Fuels* **2015**, *29* (10), 6330−6341.
(34) Rathsack, P.; Kroll, M. M.; Otto, M. Analysis of high molecular compounds in pyrolysis liquids from a german brown coal by FT-ICR-MS. *Fuel* **2014**, *115*, 461−468.
(35) McKenna, A. M.; Marshall, A. G.; Rodgers, R. P. Heavy petroleum composition. 4. Asphaltene compositional space. *Energy Fuels* **2013**, *27* (3), 1257−1267.
(36) Lababidi, S.; Panda, S. K.; Andersson, J. T.; Schrader, W. Direct coupling of normal-phase high-performance liquid chromatography to atmospheric pressure laser ionization Fourier transform ion cyclotron resonance mass spectrometry for the characterization of crude oil. *Analytical chemistry* **2013**, *85* (20), 9478−9485.
(37) McKenna, A. M.; Williams, J. T.; Putman, J. C.; Aeppli, C.; Reddy, C. M.; Valentine, D. L.; Lemkau, K. L.; Kellermann, M. Y.; Savory, J. J.; Kaiser, N. K.; et al. Unprecedented Ultrahigh Resolution FT-ICR Mass Spectrometry and Parts-Per-Billion Mass Accuracy Enable Direct Characterization of Nickel and Vanadyl Porphyrins in Petroleum from Natural Seeps. *Energy Fuels* **2014**, *28* (4), 2454−2464.
(38) Wu, Z.; Rodgers, R. P.; Marshall, A. G. ESI FT-ICR mass spectral analysis of coal liquefaction products. *Fuel* **2005**, *84* (14−15), 1790−1797. Purcell, J. M.; Merdrignac, I.; Rodgers, R. P.; Marshall, A. G.; Gauthier, T.; Guibard, I. Stepwise structural characterization of asphaltenes during deep hydroconversion processes determined by atmospheric pressure photoionization (APPI) Fourier transform ion cyclotron resonance (FT-ICR) mass spectrometry. *Energy Fuels* **2010**, *24* (4), 2257−2265.
(39) Zhang, L.; Hou, Z.; Horton, S. R.; Klein, M. T.; Shi, Q.; Zhao, S.; Xu, C. Molecular representation of petroleum vacuum resid. *Energy Fuels* **2014**, *28* (3), 1736−1749.
(40) Liu, P.; Xu, C.; Shi, Q.; Pan, N.; Zhang, Y.; Zhao, S.; Chung, K. H. Characterization of sulfide compounds in petroleum: selective oxidation followed by positive-ion electrospray Fourier transform ion cyclotron resonance mass spectrometry. *Anal. Chem.* **2010**, *82* (15), 6601−6606.
(41) Jameel, A. G. A.; Khateeb, A.; Elbaz, A. M.; Emwas, A.-H.; Zhang, W.; Roberts, W. L.; Sarathy, S. M. Characterization of deasphalted heavy fuel oil using APPI (+) FT-ICR mass spectrometry and NMR spectroscopy. *Fuel* **2019**, *253*, 950−963.
(42) Fung, B.; Khitrin, A.; Ermolaev, K. An improved broadband decoupling sequence for liquid crystals and solids. *Journal of magnetic resonance* **2000**, *142* (1), 97−101.
(43) Hendrickson, C. L.; Quinn, J. P.; Kaiser, N. K.; Smith, D. F.; Blakney, G. T.; Chen, T.; Marshall, A. G.; Weisbrod, C. R.; Beu, S. C. 21 T Fourier transform ion cyclotron resonance mass spectrometer: A national resource for ultrahigh resolution mass analysis. *J. Am. Soc. Mass Spectrom.* **2015**, *26*, 1626−1632. Smith, D. F.; Podgorski, D. C.; Rodgers, R. P.; Blakney, G. T.; Hendrickson, C. L. 21 T FT-ICR mass spectrometer for ultrahigh resolution analysis of complex organic mixtures. *Anal. Chem.* **2018**, *90* (3), 2041−2047.
(44) Robb, D. B.; Covey, T. R.; Bruins, A. P. Atmospheric pressure photoionization: an ionization method for liquid chromatography−mass spectrometry. *Anal. Chem.* **2000**, *72* (15), 3653−3659. Purcell, J. M.; Hendrickson, C. L.; Rodgers, R. P.; Marshall, A. G. Atmospheric pressure photoionization proton transfer for complex organic mixtures investigated by Fourier transform ion cyclotron resonance mass spectrometry. *J. Am. Soc. Mass Spectrom.* **2007**, *18* (9), 1682−1689.
(45) Pereira, T. M.; Vanini, G.; Oliveira, E. C.; Cardoso, F. M.; Fleming, F. P.; Neto, A. C.; Lacerda, V., Jr; Castro, E. V.; Vaz, B. G.; Romão, W. An evaluation of the aromaticity of asphaltenes using atmospheric pressure photoionization Fourier transform ion cyclotron resonance mass spectrometry−APPI (±) FT-ICR MS. *Fuel* **2014**, *118*, 348−357.
(46) Kaiser, N. K.; Savory, J. J.; Hendrickson, C. L. Controlled ion ejection from an external trap for extended *m/z* range in FT-ICR mass spectrometry. *J. Am. Soc. Mass Spectrom.* **2014**, *25*, 943−949.
(47) Kaiser, N. K.; McKenna, A. M.; Savory, J. J.; Hendrickson, C. L.; Marshall, A. G. Tailored ion radius distribution for increased dynamic range in FT-ICR mass analysis of complex mixtures. *Anal. Chem.* **2013**, *85* (1), 265−272.
(48) Chen, T.; Beu, S. C.; Kaiser, N. K.; Hendrickson, C. L. Note: Optimized circuit for excitation and detection with one pair of electrodes for improved Fourier transform ion cyclotron resonance mass spectrometry. *Rev. Sci. Instrum.* **2014**, *85* (6), No. 066107, DOI: 10.1063/1.4883179.
(49) Boldin, I. A.; Nikolaev, E. N. Fourier transform ion cyclotron resonance cell with dynamic harmonization of the electric field in the whole volume by shaping of the excitation and detection electrode assembly. *Rapid Commun. Mass Spectrom.* **2011**, *25* (1), 122−126. Kaiser, N. K.; Quinn, J. P.; Blakney, G. T.; Hendrickson, C. L.; Marshall, A. G. A Novel 9.4 T FT ICR mass spectrometer with improved sensitivity, mass resolution, and mass range. *J. Am. Soc. Mass Spectrom.* **2011**, *22* (8), 1343−1351.
(50) Blakney, G. T.; Hendrickson, C. L.; Marshall, A. G. Predator data station: A fast data acquisition system for advanced FT-ICR MS experiments. *Int. J. Mass Spectrom.* **2011**, *306* (2−3), 246−252.
(51) Savory, J. J.; Kaiser, N. K.; McKenna, A. M.; Xian, F.; Blakney, G. T.; Rodgers, R. P.; Hendrickson, C. L.; Marshall, A. G. Parts-Per-Billion Fourier transform ion cyclotron resonance mass measurement accuracy with a "Walking" calibration equation. *Anal. Chem.* **2011**, *83* (5), 1732−1736.
(52) Kendrick, E. A mass scale based on CH_2 = 14.0000 for high resolution mass spectrometry of organic compounds. *Anal. Chem.* **1963**, *35* (13), 2146−2154.
(53) Hughey, C. A.; Hendrickson, C. L.; Rodgers, R. P.; Marshall, A. G.; Qian, K. Kendrick Mass Defect Spectroscopy: A Compact Visual Analysis for Ultrahigh-Resolution Broadband Mass Spectra. *Anal. Chem.* **2001**, *73*, 4676−4681.
(54) McLafferty, F. W.; Turecek, F. *Interpretation of Mass Spectra, 4th ed.*; University Science Books, 1993. DOI: 10.1002/bms.1200230614.

https://doi.org/10.1021/acs.energyfuels.3c05200
Energy Fuels XXXX, XXX, XXX−XXX

(55) *PetroOrg. Software*; Florida State University, Omics LLC: Tallahassee, Fl, 2014. (accessed 20 Janurary 2017).
(56) Fletcher, T.; Bai, S.; Pugmire, R.; Solum, M.; Wood, S.; Grant, D. Chemical structural features of pyridine extracts and residues of the Argonne Premium coals using solid-state C-13 NMR spectroscopy. *Energy Fuels* **1993**, *7* (6), 734−742.
(57) Maroto-Valer, M. M.; Taulbee, D. N.; Andresen, J. M.; Hower, J. C.; Snape, C. E. Quantitative 13C nmr study of structural variations within the vitrinite and inertinite maceral groups for a semifusinite-rich bituminous coal. *Fuel* **1998**, *77* (8), 805−813. Choi, C.-Y.; Muntean, J. V.; Thompson, A. R.; Botto, R. E. Characterization of coal macerals using combined chemical and NMR spectroscopic methods. *Energy Fuels* **1989**, *3* (4), 528−533.
(58) Wang, Q.; Pan, S.; Bai, J.; Chi, M.; Cui, D.; Wang, Z.; Liu, Q.; Xu, F. Experimental and dynamics simulation studies of the molecular modeling and reactivity of the Yaojie oil shale kerogen. *Fuel* **2018**, *230*, 319−330.
(59) Blom, L.; Edelhausen, L.; Van Krevelen, D. W. Chemical structure and properties of coal 0.18. Oxygen groups in coal and related products. *Fuel* **1957**, *36* (2), 135−153.
(60) Kelemen, S.; Afeworki, M.; Gorbaty, M.; Sansone, M.; Kwiatek, P.; Walters, C.; Freund, H.; Siskin, M.; Bence, A.; Curry, D. Direct characterization of kerogen by X-ray and solid-state 13C nuclear magnetic resonance methods. *Energy Fuels* **2007**, *21* (3), 1548−1561.
(61) Sharma, A.; Kyotani, T.; Tomita, A. Direct observation of raw coals in lattice fringe mode using high-resolution transmission electron microscopy. *Energy Fuels* **2000**, *14* (6), 1219−1225.
(62) Derbyshire, F.; Andrews, R.; Jacques, D.; Jagtoyen, M.; Kimber, G.; Rantell, T. Synthesis of isotropic carbon fibers and activated carbon fibers from pitch precursors. *Fuel* **2001**, *80* (3), 345−356. Li, X.; Zhu, X.-q.; Okuda, K.; Zhang, Z.; Ashida, R.; Yao, H.; Miura, K. Preparation of carbon fibers from low-molecular-weight compounds obtained from low-rank coal and biomass by solvent extraction. *New carbon materials* **2017**, *32* (1), 41−47. Yang, J.; Nakabayashi, K.; Miyawaki, J.; Yoon, S.-H. Preparation of pitch based carbon fibers using Hyper-coal as a raw material. *Carbon* **2016**, *106*, 28−36.
(63) Lewis, I. C. Thermal polymerization of aromatic hydrocarbons. *Carbon* **1980**, *18*, 191−196.
(64) Sasaki, T.; Jenkins, R. G.; Eser, S.; Schobert, H. H. Carbonization of anthracene and phenanthrene. 1. Kinetics of mesophase development. *Energy Fuels* **1993**, *7* (6), 1039−1046.
(65) Murata, S.; Tani, Y.; Hiro, M.; Kidena, K.; Artok, L.; Nomura, M.; Miyake, M. Structural analysis of coal through RICO reaction: detailed analysis of heavy fractions. *Fuel* **2001**, *80* (14), 2099−2109.
(66) Herod, A. A.; Li, C.-Z.; Parker, J. E.; John, P.; Johnson, C. A. F.; Smith, G. P.; Humphrey, P.; Chapman, J. R.; Kandiyoti, R.; Games, D. E. Characterization of coal by matrix-assisted laser desorption ionization mass spectrometry. I. The Argonne coal samples. *Rapid Commun. Mass Spectrom.* **1994**, *8* (10), 808−814.
(67) Miura, K.; Shimada, M.; Mae, K.; Sock, H. Y. Extraction of coal below 350 degrees C in flowing non-polar solvent. *Fuel* **2001**, *80* (11), 1573−1582.
(68) Larsen, J. W.; Pan, C.-S.; Shawver, S. Effect of demineralization on the macromolecular structure of coals. *Energy Fuels* **1989**, *3* (5), 557−561.
(69) Herod, A. A.; Kandiyoti, R.; Parker, J. E.; Johnson, C. A. F.; John, P.; Smith, G. P.; Li, C. Z. Carbon clusters from coal-derived materials. *Rapid Commun. Mass Spectrom.* **1993**, *7* (5), 360−362.
(70) Herod, A. A.; Kandiyoti, R. Detection of high-molecular-mass materials in coal-derived liquids by independent techniques. *Fuel* **1995**, *74* (5), 784−786.
(71) Hsu, C. S.; Lobodin, V. V.; Rodgers, R. P.; McKenna, A. M.; Marshall, A. G. Compositional boundaries for fossil hydrocarbons. *Energy Fuels* **2011**, *25* (5), 2174−2178. Lobodin, V. V.; Marshall, A. G.; Hsu, C. S. Compositional space boundaries for organic compounds. *Analytical chemistry* **2012**, *84* (7), 3410−3416.
(72) Giraldo-Dávila, D.; Chacón-Patiño, M. L.; Orrego-Ruiz, J. A.; Blanco-Tirado, C.; Combariza, M. Y. Improving compositional space accessibility in (+) APPI FT-ICR mass spectrometric analysis of crude oils by extrography and column chromatography fractionation. *Fuel* **2016**, *185*, 45−58.
(73) Cho, Y.; Kim, Y. H.; Kim, S. Planar limit-assisted structural interpretation of saturates/aromatics/resins/asphaltenes fractionated crude oil compounds observed by Fourier transform ion cyclotron resonance mass spectrometry. *Analytical chemistry* **2011**, *83* (15), 6068−6073.
(74) Hower, J. C.; Eble, C. F.; O'Keefe, J. M. Phyteral perspectives: Every maceral tells a story. *International Journal of Coal Geology* **2021**, *247*, No. 103849.
(75) Purcell, J. M.; Rodgers, R. P.; Hendrickson, C. L.; Marshall, A. G. Speciation of nitrogen containing aromatics by atmospheric pressure photoionization or electrospray ionization Fourier transform ion cyclotron resonance mass spectrometry. *J. Am. Soc. Mass Spectrom.* **2007**, *18* (7), 1265−1273.
(76) Kelemen, S.; Gorbaty, M.; Kwiatek, P. Quantification of nitrogen forms in Argonne premium coals. *Energy Fuels* **1994**, *8* (4), 896−906. Kelemen, S.; Afeworki, M.; Gorbaty, M.; Kwiatek, P.; Solum, M.; Hu, J.; Pugmire, R. XPS and 15N NMR study of nitrogen forms in carbonaceous solids. *Energy Fuels* **2002**, *16* (6), 1507−1515.
(77) Kozłowski, M. XPS study of reductively and non-reductively modified coals. *Fuel* **2004**, *83* (3), 259−265.

https://doi.org/10.1021/acs.energyfuels.3c05200
Energy Fuels XXXX, XXX, XXX−XXX